PHILOSOPHICAL TRANSACTIONS OF THE ROYAL SOCIETY B BIOLOGICAL SCIENCES

Dynamics of Arthropod Filiform Hairs. I. Mathematical Modelling of the Hair and Air Motions

Joseph A. C. Humphrey, Raghuram Devarakonda, Immaculada Iglesias and Friedrich G. Barth

Phil. Trans. R. Soc. Lond. B 1993 **340**, 423-444
doi: 10.1098/rstb.1993.0083

Dynamics of arthropod filiform hairs. I. Mathematical modelling of the hair and air motions

JOSEPH A. C. HUMPHREY[1], RAGHURAM DEVARAKONDA[1], IMMACULADA IGLESIAS[1] AND FRIEDRICH G. BARTH[2]

[1]*Department of Mechanical Engineering, University of California at Berkeley, Berkeley, California 94720, U.S.A.*
[2]*Institut für Zoologie der Universität Wien, Althanstr. 14, A-1090 Wien, Austria*

CONTENTS

	PAGE
1. Introduction	424
(*a*) The problem of interest	424
(*b*) Objectives of this contribution	424
2. Modelling hair motion	424
(*a*) The geometrical approximations	424
(*b*) Equation of motion for the hair	425
(*c*) Earlier work	428
3. Modelling air flow past the hair substrate	431
(*a*) Air motion parallel to the substrate axis	432
(*b*) Air motion perpendicular to the substrate axis	433
(*c*) Experimental verification of analytical expressions for velocity	434
4. Numerical solution methodology	435
5. A method for determining the physical constants S and R	435
6. Calculated results and discussion: parameter dependence of hair motion	437
(*a*) Sensitivity to substrate–air flow relative orientation	438
(*b*) Sensitivity to variations in S and R	438
(*c*) Sensitivity to hair length and shape	440
(*d*) Phase shift between hairs in a cluster	440
References	442
Appendix 1	442
Appendix 2	443

SUMMARY

This study is concerned with the mathematical modelling of the motion of arthropod filiform hairs in general, and of spider trichobothria specifically, in oscillating air flows. Analysis of the behaviour of hair motion is based on numerical calculations of the equation for conservation of hair angular momentum. In this equation the air-induced drag and virtual mass forces driving the hair about the point of attachment to the substrate are both significant and require a correct prescription of the air velocity. Two biologically significant cases are considered. In one the air oscillates parallel to the axis of the cylindrical substrate supporting the hair. In the other the air oscillates normal to that axis. It is shown that the relative orientation between the respective directions of the air motion and the substrate axis has a marked effect on the magnitudes of hair displacement, velocity and acceleration but not on the resonance frequency of the hair. It is also shown that the variation of velocity with distance from the substrate depends on the value of the parameter $Re_S\,St_S$, the product of the Reynolds number and the Strouhal number characterizing the motion of air past the substrate. In the case of air motion parallel to the substrate axis the analytical result derived by Stokes (1851), for a fluid oscillating along a flat surface of infinite extent, applies if $Re_S\,St_S > 10$ or, equivalently, if $fD^2/\nu > 20/\pi$ where f is the air oscillation frequency, D the substrate diameter and ν the kinematic viscosity of the air. In contrast, in the case of air motion perpendicular to the substrate axis Stokes' (1851) analysis never applies due to a substrate curvature dependence of the velocity profile for all biologically significant values of $Re_S\,St_S$. Present theoretical considerations point to a new method for simultaneously determining R, the damping constant, and S, the torsional restoring constant of a filiform hair from measurements of the phase difference between hair

Phil. Trans. R. Soc. Lond. B (1993) **340,** 423–444
Printed in Great Britain

displacement and air velocity as a function of the air oscillation frequency. For the filiform hairs of crickets we find from the data available that $S = O(10^{-11})$ N m rad^{-1} and $R = O(10^{-13})$ N m s rad^{-1}. All major qualitative aspects of known hair motion in response to air motion are correctly predicted by the numerical model.

1. INTRODUCTION

(*a*) *The problem of interest*

Filiform hairs are mechanoreceptive sensilla located on the integument of various terrestrial arthropods, well known examples being crickets, cockroaches, caterpillars, spiders and scorpions. They are called trichobothria in arachnids and are found on the walking legs and pedipalps of all true spiders. As displacement transducers they are extremely sensitive to the motion of the air. The general morphology and functional properties of arthropod mechanoreceptive hair sensilla, including the trichobothria, have been summarized by Barth & Blickhan (1984) and a review of research on arachnid trichobothria has been given by Reißland & Görner (1985). These authors discuss some of the earlier work by Tautz (1977, 1979) and Reißland & Görner (1978) who have investigated the mechanoreceptive characteristics of the thoracal hairs of caterpillars and the trichobothria of web spiders, respectively.

In this study we are concerned with the mathematical modelling of the oscillatory motion of filiform hairs in all arthropods, irrespective of the fluid medium (air or water) inducing the oscillations. However, it serves the objectives of this paper to focus attention primarily on spider trichobothria oscillating in air. In a companion paper, Barth *et al.* (1993) provide details of the arrangement, fine anatomy, and mechanical properties of the trichobothria on *Cupiennius salei* spiders. As will be shown, the geometry, physical properties and flow conditions underpinning the trichobothrium model developed here can all be readily altered to accommodate the geometrical and dynamical characteristics of arbitrary hair–substrate fluid flow configurations.

(*b*) *Objectives of this contribution*

After providing the necessary theoretical background, in § 2 it will be shown in the review of earlier work that all previous attempts to model the dynamics of filiform hairs in arthropods have failed to do so in a consistent and accurate manner in spite of the availability of the necessary theory. It is the purpose of this study to redress this situation by accomplishing several related objectives. These are to:

1. Provide a consistently derived equation of motion which accurately represents the dynamics of an oscillating filiform hair. Among various requirements, the solution to this equation should account for the influence of both hair curvature and substrate curvature on hair motion.
2. Apply theoretical analysis to this equation of motion in order to delineate an experimental methodology for simultaneously determining numerical values for the restoring and damping constants, S and R of a filiform hair. The analytical results of this activity serve to identify the type and accuracy of experimental data required to determine S and R. They also allow an evaluation of the suitability of data already in the literature that could serve this purpose.
3. Outline and apply a numerical methodology for solving the equation of motion for the hair subject to accurate expressions for the velocity of the air, including the effects of substrate curvature and viscous shear. For this, we focus on the characteristics of an oscillatory motion with zero mean net flow and investigate the relevant parameters affecting hair motion.

The availability of a mathematical model accurately describing fluid-driven hair motion begs its application to investigate the response of filiform hairs exposed to fluid flow conditions of biological interest. In this regard it is of special interest to establish the connections among: (i) hair structure and physical properties; (ii) air flow stimuli; and (iii) animal behavioural response. These and related points are considered in more detail in the companion paper by Barth *et al.* (1993).

In concluding this section we note that this communication has been written with the biologist, as reader, primarily in mind. Thus, we have put more effort into clarifying all major physico-mathematical concepts necessary for understanding the model than would be required by a more mathematically oriented readership. This, we hope, will encourage and assist biologists to use the model with confidence. Throughout the paper we distinguish between the meanings attributed to 'analytical procedures or results' and 'numerical procedures or results'. By the former we refer to the application of theoretical procedures that allow the derivation of analytical solutions in closed form for the equations of interest; that is, completely general solutions expressible purely in terms of, for example, algebraic and transcendental functions. By the latter we mean the application of finite difference procedures, encoded in the form of computer algorithms, that yield specific numerical solutions for the same or related equations.

2. MODELLING HAIR MOTION

(*a*) *The geometrical approximations*

The insert in figure 1, from Barth *et al.* (1993), shows typical arrangements of trichobothria on a segment of the meta-tarsus of a *Cupiennius salei* spider leg. Only the trichobothria are shown but, in reality, each trichobothrium projects at about 90° to the leg surface through a dense arrangement of relatively stiff hairs

PHILOSOPHICAL TRANSACTIONS OF THE ROYAL SOCIETY B BIOLOGICAL SCIENCES

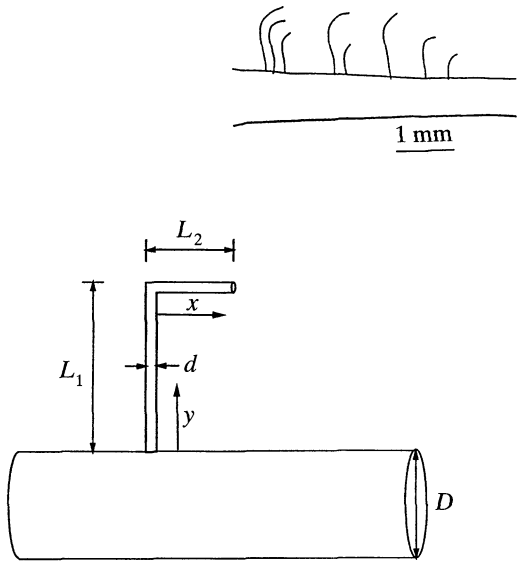

Figure 1. Showing the geometrical approximation made in this study to model the motion of a curved trichobothrium of diameter d projecting from a *Cupiennius salei* spider leg of diameter D. For a straight hair $L_2 = 0$. The insert, from Barth *et al.* (1992), shows typical arrangements of trichobothria on a segment of the meta-tarsus of a *Cupiennius* spider.

which are insensitive to air motion and which possess other functions such as tactile or chemoreceptive. In addition to innervated cuticular hairs, a carpet of small non-innervated hairs covers the spider integument.

Both the trichobothria clusters and the individual sensilla composing them present clearly recognizable and repeatable structural patterns. The dorsal view of an entire spider leg, provided in Barth *et al.* (1993), shows that along its length the trichobothria clusters on the tarsus and metatarsus, as well as some trichobothria on the tibia, are contained in a common plane which passes through the longitudinal axis of the leg. From base to tip, the hairs range in length between 100 and 1500 μm, approximately. In each cluster the hairs are arranged so that the longest are located distally along the leg. The longest hairs are also the most strongly curved at the tip, with the tip of the hair always directed proximally. Individual hair diameters vary, from a maximum at the base of the hair to a minimum at the tip, giving the hairs the appearance of elongated curved cones. Average hair diameters range from 5 μm for the short hairs to 15 μm for the long. This yields values of hair length to diameter ratios, L/d, ranging between 20 and 100. The distance between hairs ranges from about 50 to 500 μm for the clusters located on the meta-tarsus and tibia. This yields values of hair spacing to diameter ratios, α/d, ranging between 10 and 100, approximately.

For the purposes of this paper, which emphasizes the mathematical modelling of the air-driven motion of filiform hairs in general, and trichobothria in particular, it is necessary to define a simplified geometry representing a single hair and its substrate. Figure 1 shows the geometrical approximation made in this study for a curved trichobothrium projecting from a *Cupiennius salei* leg of diameter D. The entire hair unit is deflected about the point of attachment to the substrate when driven by air oscillations. The hair is modelled as an inflexible smooth cylinder of constant effective diameter d, with a right-angle bend near its tip in order to capture the qualitative influence of hair curvature on hair motion. The sum of the two lengths of this cylinder, $L_1 + L_2$, is equal to the total length, L, of the real hair. The cylindrical model for the hair may be taken as solid or as hollow, with all solid portions of the hair assumed to be homogeneous and of density $\rho_{\text{hair}} = 1100\ \text{kg m}^{-3}$ (Shimozawa & Kanou 1984).

The immobile leg supporting the hair is also approximated as a cylinder, but of much larger diameter than the hair. The precise topological details of the various hairs on the leg are ignored when assessing the influence of the leg on the air flowing past it. Instead, the leg and its hairy surface are combined into an equivalent cylindrical substrate of effective diameter, D. This means that the substrate is viewed as a smooth cylinder in so far as a filiform hair projecting from it is concerned. Typically, Barth *et al.* (1993) find $D/d = 200$, for an adult *Cupiennius salei*.

For a straight hair, such as a filiform hair on a cricket cercus, we would take $L_2 = 0$ in the present geometrical model and, if it were shown to be critical, the hair would be approximated as a cone instead of a cylinder to find its moment of inertia. However, such a practice introduces a modelling inconsistency present in earlier works such as, for example, Fletcher (1978) and Shimozawa & Kanou (1984) which we have chosen to avoid. Relatively simple analytical relations from which to calculate the stress-induced fluid forces acting on a cone as a function of its length are not known as they are for a cylinder. Therefore, it is more consistent to model the hair as a cylinder of effective or average diameter, d, for the determination of both the fluid forces and the moment of inertia. The notion of an effective diameter is also consistent with the following separate consideration. For the low values of the Reynolds number typical of hair motions ($Re \ll 1$, with Re as defined in equation (5)), the detailed topological characteristics of the structures composing the hair surface are unimportant for determining the hair's moment of inertia and the bulk fluid forces acting upon it as long as the structures are evenly distributed and the spaces between them are smaller than the structures themselves; that is, as long as the structures are uniformly and closely packed. Close packing, as found in trichobothria (see Barth *et al.* 1993), precludes any significant fluid motion in the spaces between structures thus allowing any hair to be viewed as a smooth cylinder of effective diameter d.

(*b*) *Equation of motion for the hair*

For the discussion of earlier work, and for the numerical calculation of hair motion in this study, the principle of the conservation of angular momentum is applied to the geometry approximating a bent filiform hair with respect to the point about which it oscillates

PHILOSOPHICAL TRANSACTIONS OF THE ROYAL SOCIETY B BIOLOGICAL SCIENCES

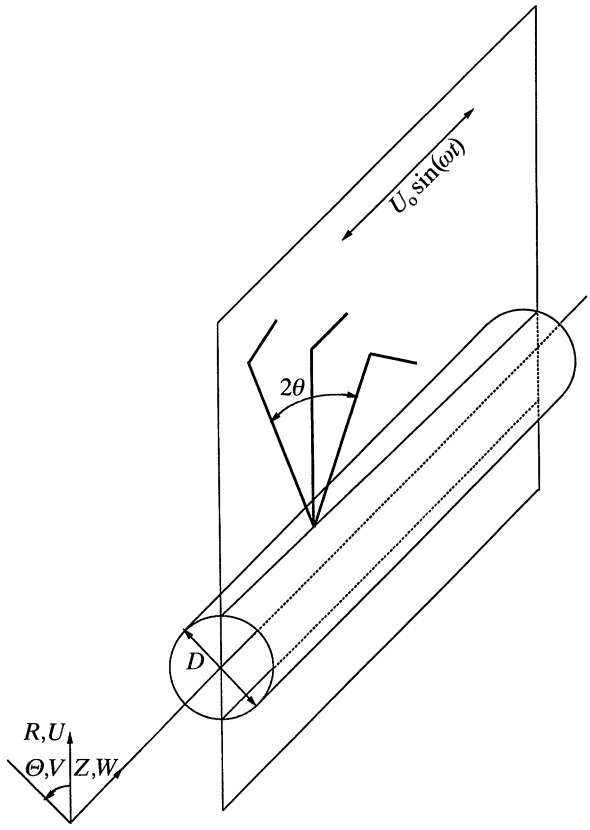

Figure 2. Configuration for the case of air flow oscillating parallel to the longitudinal axis (Z-axis) of the spider leg. The coordinate system and velocity components are as indicated although, in this case, the radial (U) and circumferential (V) velocity components are respectively zero.

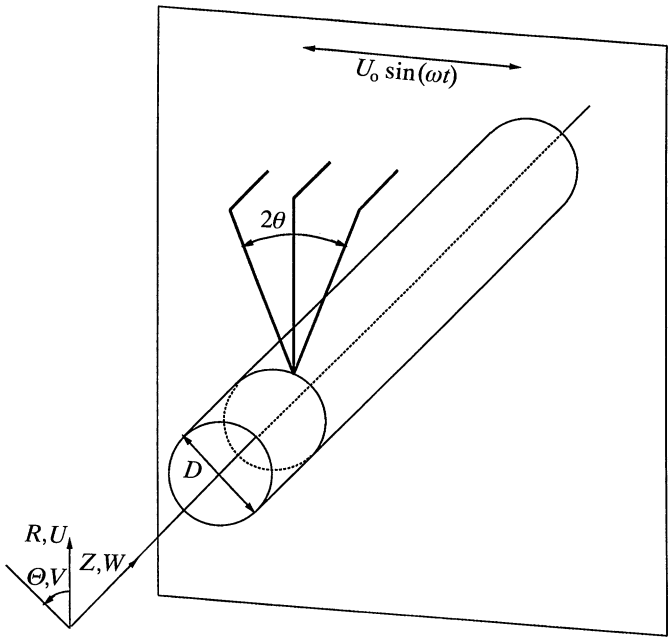

Figure 3. Configuration for the case of air flow oscillating perpendicular to the longitudinal axis (Z-axis) of the spider leg. The coordinate system and velocity components are as indicated although, in this case, the longitudinal (W) velocity component is zero.

on the substrate. Two biologically meaningful situations of fundamental interest are shown in figures 2 and 3. Figure 2 corresponds to an air flow oscillating parallel to the longitudinal axis (Z-axis) of the substrate. Figure 3 corresponds to an air flow oscillating perpendicular to that axis. The angular displacements, θ, shown for the hairs in these two figures are exaggerated because, generally, $\theta < 10°$ suffices to stimulate action potentials in spiders (Barth *et al.* 1993) and $\theta < 1°$ suffices to stimulate action potentials in crickets (Shimozawa & Kanou 1984).

In both of the configurations shown in figures 2 and 3 the conservation of angular momentum for the hair is given by

$$I\ddot{\theta} = -R\dot{\theta} - S\theta + T_{\mathrm{D}} + T_{\mathrm{VM}}, \qquad (1)$$

where I (N m s^2 rad^{-1}) is the moment of inertia of the hair with respect to the axis of rotation, R (N m s rad^{-1}) is the damping constant, S (N m rad^{-1}) is the torsional restoring constant, θ (rad) is the angular displacement of the L_1 cylinder segment attached to the substrate with respect to its equilibrium orientation, and the superscript dots over θ denote differentiation with respect to time.

Equation (1) is the equation of motion for a simple forced damped harmonic oscillator and it provides the theoretical foundation underpinning the numerical model for hair motion in the present study. In simpler forms it has been used by Fletcher (1978) and Shimozawa & Kanou (1984) for the same purpose. Equation (1) states that the rate of change of angular momentum of the hair is due to four contributions composing the total torque acting upon it. In order of appearance on the right hand side of the equation these are: (i) the frictional torque, arising at the rotation point of the hair; (ii) the restoring torque, also arising at the rotation point of the hair; (iii) the torque, T_{D}, arising due to fluid-induced stress forces (form and frictional drag) acting along the length of the hair; and (iv) the torque, T_{VM}, associated with the added (or virtual) mass of fluid (for the trichobothria, air) which at any instant must be accelerated along with the hair. Of these torques, the first two always work to oppose hair deflection.

The quantities R and S in equation (1) must be obtained from experimentation with real hairs and we discuss how this can be achieved in § 5. The moment of inertia, I, of the hair is most conveniently evaluated using the parallel axis theorem. For homogeneously solid hairs the expressions required are:

1. For the hair in the configuration of figure 2, corresponding to the fluid oscillating parallel to the longitudinal axis of the cylindrical substrate:

$$I = (\pi\rho_{\mathrm{hair}} d^2/48)\,(L_1\,(4L_1^2 + (3/4)\,d^2) + L_2(12\,L_1^2 + (3/4)\,d^2 + L_2^2)). \qquad (2a)$$

2. For the hair in the configuration of figure 3, corresponding to the fluid oscillating perpendicular to the longitudinal axis of the cylindrical substrate:

$$I = (\pi\rho_{\mathrm{hair}} d^2/48)\,(L_1\,(4\,L_1^2 + (3/4)\,d^2) + L_2\,(12\,L_1^2 + (3/2)\,d^2)). \qquad (2b)$$

The moments of inertia for hollow hairs are also given by equations (2a,2b) if one subtracts from them identical expressions wherein the quantity d is substituted for d_{in}, the inner diameter corresponding to the hollow portion of the hair.

The torques T_D and T_{VM} are obtained by integrating the fluid-induced drag and added mass forces acting along the total length, $L = L_1 + L_2$, of the hair. Calling F_D and F_{VM} the drag and added mass forces per unit length respectively acting on the hair, it follows that

$$T_D = \int_0^{L_1} F_D\, y\, dy + \int_0^{L_2} F_D\, L_1\, dx, \tag{3}$$

and

$$T_{VM} = \int_0^{L_1} F_{VM}\, y\, dy + \int_0^{L_2} F_{VM}\, L_1\, dx. \tag{4}$$

The forms of equations (3) and (4) imply that the drag and added mass forces respectively acting on the L_1 and L_2 segments of the hair are additive and that flow field interference effects where the two segments join are negligible. The assumption is reasonable as long as both $L_1/d \gg 1$ and $L_2/d \gg 1$ as in the case of many trichobothria (Barth *et al.* 1993).

Together with appropriately specified physical properties and initial conditions, equations (1–4) determine the motion of a bent hair, or of a straight hair when $L_2 = 0$. Experimentally validated theoretical expressions for F_D and F_{VM}, applicable to a fluid oscillating perpendicular to the L_1 and L_2 segments of a hair have been derived by Stokes (1851). Corresponding expressions applicable to a fluid oscillating parallel to the L_2 segment of a hair have been derived by us (and others).

The main constraints to be satisfied in Stokes' (1851) theory for a fluid oscillating perpendicular to a cylinder are that the cylinder length to diameter ratio should be $L/d \gg 1$, and that the Reynolds number of the flow at any location along the cylinder, defined here as

$$Re = V_r\, d/2\, \rho/\mu, \tag{5}$$

should be $Re \ll 1$. Of these two constraints only the first applies to the theory for a fluid oscillating parallel to a cylinder provided the motion remains laminar. Using the data for trichobothria in Barth *et al.* (1993) and that for the filiform hairs of crickets in Kämper & Kleindienst (1990), we have verified that these constraints are readily satisfied for all the hair and air flow conditions of interest to this study. In equation (5), d is the hair diameter while ρ and μ are the fluid density and dynamic viscosity, respectively. In this study the values $\rho = 1.1774\ \mathrm{kg\ m^{-3}}$ and $\mu = 1.8462\ 10^{-5}\ \mathrm{kg\ m^{-1}\ s^{-1}}$, corresponding to air at 27°C, have been used throughout. (The symbol for the kinematic viscosity, $\nu = \mu/\rho$, is also used in this paper.) The quantity $V_r = V_F - V_C$ is the local relative velocity given by the difference between the fluid velocity, V_F, and the velocity of the cylinder itself, $V_C = y\ \dot{\theta}$, at any position along its length. It is important to note the following. For the L_1 cyclindrical hair segments shown in figures 2 and 3, and for the L_2 segment shown in figure 3, V_F is the component of fluid velocity perpendicular to those segments. For the L_2 segment shown in figure 2, V_F is the component of fluid velocity parallel to L_2. In practice, for small angular displacements of the hairs ($\theta < 10°$) V_F is essentially the component of fluid velocity parallel to the substrate at the position in question.

1. For the case of a fluid oscillating perpendicular to a cylindrical hair segment: the expressions derived for F_D and F_{VM} by Stokes (1851) are

$$F_D = 4\, \pi\, \mu\, G\, V_r, \tag{6}$$

and

$$F_{VM} = -\,(\pi\, \mu\, G\, \dot{V}_r/2\, g\, f) + \pi\rho\, (d/2)^2\, \dot{V}_r. \tag{7}$$

In these expressions $\dot{V}_r$ is the time rate of change of V_r at any position along the length of the hair and f is the frequency of flow oscillation, in Hz. For values of the dimensionless parameter

$$s = (d/4)\, (2\pi f/\nu)^{\frac{1}{2}}, \tag{8}$$

such that $s \ll 1$, Stokes (1851) shows that

$$g = 0.577 + \ln s, \tag{9}$$

and

$$G = -\,g/(g^2 + (\pi/4)^2). \tag{10}$$

Using the value of ν for air at 27°, and of d for the trichobothria of spiders (Barth *et al.* 1993) and the filiform hairs of crickets (Kämper & Kleindienst 1990) it is readily shown that the requirement that $s \ll 1$ will be satisfied as long as $f \ll 10^5$ Hz. Also, for conditions involving oscillating air flows, the second term on the right hand side of equation (7) is generally much smaller that the first. However, such is not the case for hairs oscillating in water as its density is about 1000 times that of air. Because we are interested in a generally applicable model, the second term has been retained in the numerical formulation.

2. For the case of a fluid oscillating parallel to a cylindrical hair segment: expressions for F_D and F_{VM} have been derived in the same way as done by Stokes (1851), from the velocity distribution obtained in § 3*a*. The analysis in § 3*a* is for a flow oscillating parallel to a very long cylinder of diameter D. The results also apply to the flow oscillating parallel to a cylindrical hair segment of length L_2 and diameter d if $L_2/d \gg 1$. The expressions required are

$$F_D = 2\pi\, \mu\, \mathrm{REAL}\left(\lambda\, \frac{K_1(\lambda)}{K_0(\lambda)}\, V_r\right), \tag{11}$$

and

$$F_{VM} = -\,\frac{\mu}{f}\, \mathrm{REAL}\left(i\lambda\, \frac{K_1(\lambda)}{K_0(\lambda)}\, \dot{V}_r\right), \tag{12}$$

where $\lambda = 2\, s\, i^{1/2}$, $i = (-1)^{1/2}$ is the imaginary unit and REAL denotes the real part of the expression in complex notation contained in the parentheses. The

quantities K_0 and K_1 are modified Bessel functions of the second kind which can be evaluated from series expressions available in, for example, Abramowitz & Stegun (1970).

With the above expressions for F_D and F_{VM}, equation (1) can be rewritten in a form better suited for calculating the configurations shown in figures 2 and 3, respectively. The result is

$$(I + I_1 + I_2)\,\ddot{\theta} + (R + R_1 + R_2)\,\dot{\theta} + S\,\theta = \left(\int_0^{L_1} D_1\, V_F\, y\, \mathrm{d}y + D_2\, V_F|_{y=L_1}\, L_1\, L_2\right) + \left(\int_0^{L_1} VM_1 \dot{V}_F\, y\, \mathrm{d}y + VM_2\, \dot{V}_F|_{y=L_1}\, L_1\, L_2\right), \quad (13)$$

where the symbol '$|_{y=L_1}$' means 'evaluated at $y=L_1$'. The other new symbols in equation (13) are defined as follows:

1. For the hair in the configuration of figure 2, corresponding to the fluid oscillating parallel to the longitudinal axis of the cylindrical substrate:

$$I_1 = -\pi\mu G L_1^3/6\, gf + \pi\rho (d/2)^2 L_1^3/3, \qquad I_2 = -(\mu L_1^2 L_2/f)\ \mathrm{REAL}\,[ik],$$
$$R_1 = 4/3\,\pi\mu G L_1^3, \qquad R_2 = 2\pi\mu L_1^2 L_2\ \mathrm{REAL}\,[k],$$
$$D_1 = 4\pi\mu G, \qquad D_2 = 2\pi\mu\ \mathrm{REAL}\,[k],$$
$$VM_1 = -\pi\mu G/2\, gf + \pi\rho (d/2)^2, \qquad VM_2 = -(\mu/f)\ \mathrm{REAL}\,[ik]. \quad (14)$$

where

$$k = \frac{\lambda K_1(\lambda)}{K_0(\lambda)}$$ with λ, K_0 and K_1 as defined above.

2. For the hair in the configuration of figure 3, corresponding to the fluid oscillating perpendicular to the longitudinal axis of the cyclindrical substrate:

$$I_1 = -\pi\mu G L_1^3/6\, gf + \pi\rho (d/2)^2 L_1^3/3, \qquad I_2 = -\pi\mu G L_1^2 L_2/2\, gf + \pi\rho (d/2)^2 L_1^2 L_2,$$
$$R_1 = 4/3\,\pi\mu G L_1^3, \qquad R_2 = 4\pi\mu G L_1^2 L_2,$$
$$D_1 = 4\pi\mu G, \qquad D_2 = 4\pi\mu G,$$
$$VM_1 = -\pi\mu G/2\, gf + \pi\rho (d/2)^2, \qquad VM_2 = -\pi\mu G/2\, gf + \pi\rho (d/2)^2. \quad (15)$$

In equations (13–15) the quantities subscribed '1' pertain to segment L_1 of the hair and the quantities subscribed '2' pertain to segment L_2. Specifically, I_1 and I_2 represent moments of inertia associated with the added masses of fluid moving with the L_1 and L_2 segments of a hair, respectively. Similarly, the R_1 and R_2 terms have been written to appear as additional damping factors associated with viscous fluid forces acting on these segments.

Together with the quantities defined by equations (14) and (15), equation (13) will simulate hair motion accurately provided the hair can be represented by an effective cylinder of total length L and diameter d such that $L/d \gg 1$ and $Re \ll 1$. These requirements are readily satisfied for all the filiform hairs and flow conditions of interest to this work. It is tacitly assumed that the flow past the hair retains a two-dimensional character all the way to its base. While we know that this is not true, because the velocity and acceleration of the air at the base of the hair are very small, and therefore the associated flow-induced contributions to the torque also small, the departure from two-dimensionality can be safely ignored.

(c) *Earlier work*

It appears that Tautz (1977) was the first to propose the idea of modelling filiform hairs as forced damped harmonic oscillators for establishing the dynamic characteristics of thoracal hairs in caterpillars. He did not perform a torque balance along the lines of equation (1) to determine the precise form of hair motion. Instead, he used theoretical concepts pertaining to externally forced damped harmonic motion to interpret measurements of hair and air element displacements versus frequency. From his analysis Tautz (1977) concluded that the ratio of hair tip displacement to air element displacement is two, at most, at a hair resonance frequency of 100 Hz, approximately. Experimentally, he established that at about this frequency the motion of a hair lags that of the air by approximately 90°. From his measurements Tautz (1977) also indirectly confirmed the constancy of the torsional restoring constant, S, for hair deflection angles $\theta < 10°$, but neither S nor the damping constant, R, were determined.

In his study, Tautz (1977) did not concern himself with the fluid forces due to drag and added mass acting on a hair. In fact, he claimed . . . 'It is not possible to determine the nature of the driving force theoretically for a hair vibrating in air.' We now know that this statement is incorrect. Although Tautz's (1977) analysis does not allow the establishment of a direct connection between oscillating air motion and the mechanical behaviour of the hairs which the air

motion affects, it is seminal for two reasons: (i) it establishes the biological significance of air medium vibration reception by filiform hairs in caterpillars, which are mechanically tuned to a frequency range of biological importance; and (ii) it points the way for the mathematical modelling of hair motion in general, as discussed next.

Fletcher (1978) and Shimozawa & Kanou (1984) have developed mathematical models of hair motion based on refined interpretations of Tautz's (1977) externally forced damped harmonic oscillator concept. These studies have respectively served as bases for interpreting some of the findings in subsequent investigations performed by Tautz (1979), Kämper & Kleindienst (1990) and others. Both Fletcher (1978) and Shimozawa & Kanou (1984) improved upon Tautz's (1977) model by making the driving force in the equation of motion for the hair a function of the characteristics of an oscillatory motion with zero mean net flow. However, there are some noteworthy differences between these two studies and, unfortunately, both appear to have incurred serious errors or invoked unnecessary limitations which significantly affect the validity and usefulness of their respective results. Notwithstanding, the modelling concepts advanced by these authors have greatly benefited the present investigation.

In attempting to explain some of the finer features of Tautz's (1977) data, Fletcher (1978) modelled the fluid mechanics aspects of oscillatory hair motion approximating the hair as a cone to obtain its moment of inertia. However, he applied a drag relation appropriate to a straight cylinder to evaluate the fluid forces associated with the viscosity and inertia of the air medium. The latter is precisely the problem on the motion of pendulums solved much earlier by Stokes (1851) in the classical paper referred to in § 2*b*. In Fletcher's (1978) study the hair was taken to oscillate about a point on a flat substrate with the direction of the air oscillations aligned parallel to the substrate. However, the substrate was presumed to have no viscous damping effect on the air motion. This was equivalent to specifying a 'slip' boundary condition for velocity at the air-substrate interface which, although incorrect, conveniently allowed the imposition of a spatially homogeneous time dependent air velocity profile.

In principle, Fletcher's (1978) theoretical analysis is based on equation (13) with $L_2 = 0$. Fletcher (1978) used the results from Stokes' (1851) analysis for the values of F_D and F_{VM} given by equations (6) and (7), but he omitted a factor of 2π in equation (6) and incorrectly took $F_D = 2\,\mu\, V_r\, G$ which affects the analytical results subsequently derived. The magnitude of the 2π error can be appreciated by noting that the inclusion of this factor in Fletcher's (1978) analysis yields $\delta_o = -8.9°$ (instead of 45°) for the value of the angle characterizing the phase lag between the forcing function and the air velocity as defined by Fletcher (1978). Another important consequence of correcting the 2π error is that Fletcher's (1978) approach will then yield a factor of 1.5, instead of 2, for the ratio of hair tip displacement to air element displacement for a hair forced to oscillate at or near to the value of its undamped natural frequency. Finally, we note that detailed numerical calculations performed by us (not provided here) show that the omission of the 2π factor incurs serious quantitative errors in the shapes and magnitudes of the profiles for hair displacement, velocity and acceleration when plotted as a function of the forcing function frequency.

In an attempt to represent the damping effects of viscosity on the shape and magnitude of the velocity profile, V_F, for the air oscillating along the substrate, Shimozawa & Kanou (1984) adapted the solution of Stokes' (1851) 'second problem' for the viscous motion of a fluid near an oscillating flat surface of infinite extent to the hair-substrate systems of interest to them, i.e. filiform hairs on the cerci of crickets. Panton (1984) provides a useful summary of Stokes' second problem as well as a proof concerning the adaptation of its solution to the converse problem of a fluid oscillating near a fixed flat surface. The analysis shows that for a fluid oscillating parallel to and far away from a flat surface with velocity $U_o \sin(\omega t)$ (where U_o is the amplitude of the flow oscillation, $\omega = 2\pi f$ is the frequency in radians per second of the flow oscillation, and t is time) the instantaneous dimensionless fluid velocity, at time t and at a distance y perpendicular to the surface, is given by

$$V_{St} = v/U_o = (\sin(\omega t) - \sin(\omega t - \beta y)\, e^{-\beta y}), \qquad (16)$$

where $\beta = (\omega/2\nu)^{1/2}$ is a system parameter with dimensions m^{-1}. The location $y = \delta_{St}$ from the surface where viscous damping is detected as a 1% reduction in the amplitude of the far field velocity oscillation is given by

$$\delta_{St} = 4.5/\beta = 4.5(\nu/\pi f)^{1/2}. \qquad (17)$$

Setting ν for air at 27°C, equation (17) yields $\delta_{St} = 1006\ \mu m$ for $f = 100$ Hz and $\delta_{St} = 450\ \mu m$ for $f = 500$ Hz. From these results we anticipate that the variation in the shape of the velocity profile with y, due to substrate-induced viscous damping of air motion, will affect the magnitudes of the drag and added mass forces acting on hairs shorter than about 450 μm when $f < 500$ Hz, or acting on hairs shorter than about 1000 μm when $f < 100$ Hz. The ways by which substrate curvature and the presence of other hairs can alter this finding are discussed in § 3.

The equation used by Shimozawa & Kanou (1984) to model hair motion is also equation (13) with $L_2 = 0$ and the following restrictions:

1. The hair is approximated as a cone to calculate the moment of inertia and as a cylinder to calculate the drag.
2. All terms in the equation associated with the added mass were neglected. This is equivalent to neglecting the entire contribution of T_{VM} to the balance expressed by equation (1).
3. The frequency dependence embedded in the coefficient G associated with the drag force, F_D, was ignored. Instead, the authors assumed a pseudo-steady flow past the hair and invoked an Oseen

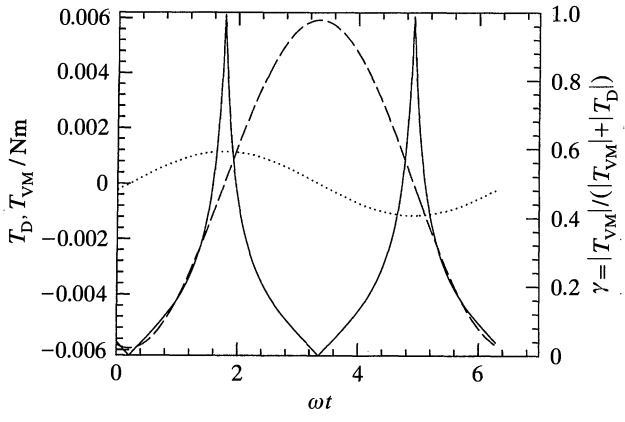

Figure 4. Plots of the virtual mass (T_{VM}) (dotted line) and viscous drag (T_D) (dashed line) torques, and of the ratio γ (solid line) over one period of air motion at $f = 100$ Hz and $U_o = 5$ mm s^{-1} for a straight solid hair with $d = 7$ μm, $L_1 = 500$ μm, $S = 4 \times 10^{-12}$ N m rad^{-1} and $R = 0$.

relation for calculating the viscous drag. (The reader is referred to White (1991) for an explanation of the Oseen flow approximation.)

4. By adapting the solution to Stokes' (1851) second problem to the hair-substrate pair, the authors precluded advancing any understanding of the influence of substrate curvature on the motion of the air and, consequently, on the motion of the hair.
5. Experimentally determined values were used for the torsional restoring constant, S, but, as in Fletcher's (1978) work, $R = 0$ was assumed for the damping factor inherent to the hair. Thus, the detailed effects of this parameter on hair motion remain unexplored.

We now comment on the effects of restrictions 2 and 3 on the prediction of hair motion. (The effects of removing restrictions 4 and 5 are more appropriately illustrated and discussed in § 6.) The general question, implied in Tautz's (1979) study, concerning the relative importance of all the forces (or torques) affecting hair motion is then addressed. We note that various errors in the paper by Shimozawa & Kanou (1984) were subsequently clarified in the paper by Kämper & Kleindienst (1990).

(i) *The importance of the virtual mass torque*

The fallacy of neglecting the contribution of T_{VM} to the balance expressed by equation (1) is best demonstrated by performing numerical calculations with and without this term in the model. We have done this and conclude that for conditions of biological interest, both in air and water, the neglect of T_{VM} induces significant errors in the calculations of the magnitudes of hair displacement, velocity and acceleration, respectively. Theoretical considerations readily show why this is the case.

Equation (13) admits an analytical solution (see Appendix 1) for the angular displacement, θ, of a straight hair projecting perpendicular to a flat substrate immersed in an oscillating air flow with velocity distribution given by equation (16). This is precisely the problem solved numerically by Shimozawa & Kanou (1984), but neglecting the added mass terms which we have retained. With analytical expressions available for V_F and θ as a function of the relevant parameters it is a simple matter to obtain corresponding expressions for T_{VM} and T_D, provided in Appendix 1. Plots of these two quantities and of the ratio $\gamma = |T_{VM}|/(|T_{VM}| + |T_D|)$ are shown in figure 4. The plots cover one period of motion for a typical solid filiform hair oscillating at $f = 100$ Hz in a sinusoidal air flow field with $U_o = 5$ mm s^{-1}. The results reflect the well known fact that the drag and virtual mass forces, F_D and F_{VM}, are out of phase by 90°. They also show that over most of the oscillation cycle $\gamma > 10\%$. From this and additional calculations for conditions of biological interest, in both air and water, we conclude that it is indispensable to retain the contribution of T_{VM} to equation (1) if a physically accurate representation of hair motion is to be achieved.

(ii) *The dependence of drag on flow oscillation frequency*

To show the importance of retaining the frequency dependence embedded in the coefficient G associated with the drag force F_D, it is convenient to work with the definition of the drag coefficient for a very long straight cylinder ($L/d \gg 1$) in the perpendicular flow orientation as given by Panton (1984),

$$C_D = F_D/d/(1/2\ \rho\ V_r^2). \tag{18}$$

Substitution of equation (6) for F_D into equation (18) yields

$$C_{D(Stokes)} = 16\pi G/Re \tag{18a}$$

for the case of an oscillating flow. In contrast, for a steady Oseen flow (White 1991) gives

$$C_{D(Oseen)} = (16\pi/Re)\ (1/2 - 0.577 + \ln(16/Re))^{-1}. \tag{18b}$$

The quantity G in equation (18a) is given by equation (10). It is a function of g, given by equation (9), which can be rewritten as

$$g = 0.577 + 1/2 \ln(Re\ St/4). \tag{9a}$$

In equation (9a) $St = \omega\ d/2/V_r$ is the Strouhal number of the cylinder which, like Re, is based on the velocity of the fluid relative to that of the cylinder. Thus, $C_{D(Stokes)} = f(Re, St)$ while $C_{D(Oseen)} = f(Re)$.

Figure 5 shows plots of these two coefficients as a function of St for $Re = 0.02$ and 0.002, respectively. The results illustrate that: (i) for any $St > 0$, the difference between these two drag coefficients increases as Re decreases, (ii) for very small non-zero values of St, the values of these two coefficients approach the same limit. For the hairs and flow conditions of interest here and in Shimozawa & Kanou (1984) we find the following approximate ranges for St and Re: $0.1 < St < 1.0$ and $0.001 < Re < 0.02$. For $St = 1.0$ and $Re = 0.002$ an Oseen flow assumption would incur an error of about 50% in the C_D coefficient and, hence, in the magnitude of the associated drag force. The corresponding error for $Re = 0.02$ is similar. Therefore, except for $St \ll 1$, the assumption of a steady Oseen flow relation is unjusti-

PHILOSOPHICAL TRANSACTIONS OF THE ROYAL SOCIETY B BIOLOGICAL SCIENCES

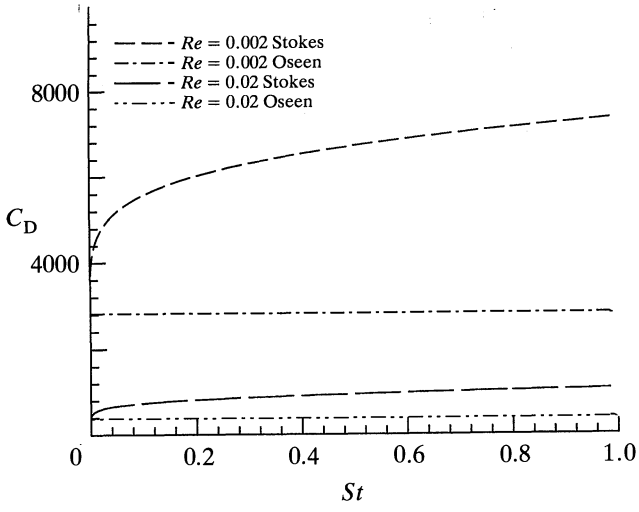

Figure 5. Plots of the drag coefficient (C_D) for cylinders in oscillating Stokes flow and steady Oseen flow, $C_{D(Stokes)}$ and $C_{D(Oseen)}$ in the text, as functions of the Strouhal number (St) for two values of the Reynolds number: $Re = 0.002$ and $Re = 0.02$.

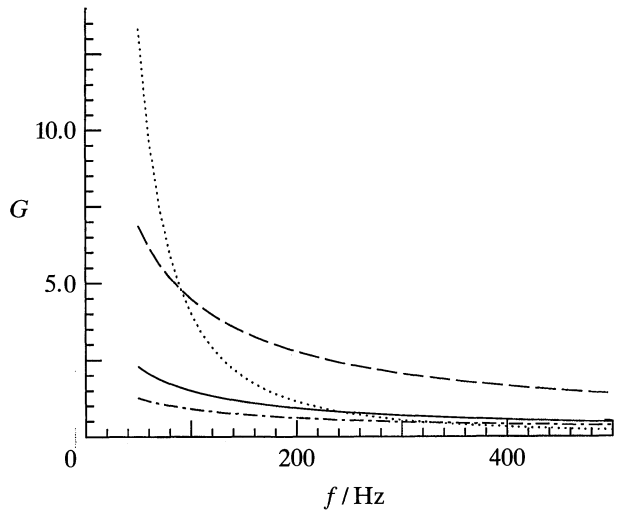

Figure 6. Plots of the dimensionless groups in equation (19) as functions of frequency with $U_0 = 5$ mm s^{-1} for a straight solid hair with $d = 7$ μm, $L_1 = 500$ μm, $S = 4 \times 10^{-12}$ N m rad^{-1} and $R = 0$. G_R, solid line; G_S, dotted line; G_D, dashed line; G_{VM}, dot-dashed line.

fied for calculating the drag force on a filiform hair in an oscillating flow field.

(iii) *Relative importance of the torques affecting hair motion*

To establish the relative importance of all the torques affecting hair motion, it is instructive to recast equation (13) in dimensionless form. We do this for a straight hair in order to obtain a general result. Define $I_{eff} = I + I_1$ and $R_{eff} = R + R_1$, and use ω^{-1} to scale time, $L = L_1$ to scale linear dimensions, the imposed oscillating air flow amplitude (U_o) to scale linear velocity, and the quantity $U_o/L\,\omega$ to scale the angular dimensions in θ, $\dot{\theta}$, and $\ddot{\theta}$. The result is

$$\ddot{\theta}^* + \frac{R_{eff}}{I_{eff}\,\omega}\,\dot{\theta}^* + \frac{S}{I_{eff}\,\omega^2}\,\theta^* = \frac{4\pi\,\mu\,G\,L^3}{I_{eff}\,\omega}\left(\int_0^{L_1^*} V_F^*\,\eta\,d\eta\right) - \frac{\pi_2\,\mu\,G\,L^3}{I_{eff}\,\omega\,g}\left(\int_0^{L_1^*} V_F^*\,\eta\,d\eta\right), \quad (19)$$

where $\eta = y/L$, $L_1^* = L_1/L$, $V_F^* = V_F/U_o$, $\dot{V}_F^* = \dot{V}_F/(\omega U_o)$, $\theta^* = \theta\,L\,\omega/U_o$, $\dot{\theta}^* = \dot{\theta}\,L/U_o$, $\ddot{\theta}^* = (\ddot{\theta}\,L)/(\omega\,U_o)$, with dimensionless time in the differentiated terms taken as $\tau = \omega t$.

Equation (19) reveals that, in general, the notion of an oscillating hair is characterized by the following four dimensionless groups:

$$G_R = R_{eff}/I_{eff}\,\omega, \qquad G_s = S/I_{eff}\,\omega^2, \qquad G_D = 4\,\pi\,\mu\,G\,L^3/I_{eff}\,\omega, \qquad G_{VM} = -\,\pi^2\,\mu\,G\,L^3/I_{eff}\,\omega\,g. \quad (20)$$

The scaling used to obtain equation (19) ensures that the quantities which the dimensionless groups respectively multiply are all of order unity. Thus, an evaluation of the magnitudes of the dimensionless groups respectively associated with these terms will establish their relative importance. Figure 6 provides such a comparison as a function of frequency for a typical filiform hair and flow conditions. (In the calculations we have set $R = 0$ since this quantity is not yet known. We later find that the value of R is of the order of R_1 and R_2 so that taking $R = 0$ does not affect the order of magnitude of G_R.) Contrary to the assumptions made by Fletcher (1978) and Shimozawa & Kanou (1984), these results show that over the biological range of frequencies ($f = 10$–500 Hz) none of the terms in equation (19) is negligible relative to the rest and all must be accounted for in an accurate analysis of hair motion.

3. MODELLING AIR FLOW PAST THE HAIR SUBSTRATE

The solution of equation (13) requires expressions for the components of air velocity and acceleration affecting hair motion. To find these quantities it is necessary to solve for the flow field oscillating about the fixed cylindrical substrate (the spider leg or cricket cercus) supporting the hair. We tacitly assume that this flow field is not affected by the presence of the filiform hairs projecting from the substrate. However, to be consistent with the conditions allowing the use of equations (6,7) and (11,12) for F_D and F_{VM}, one must ask if the hairs in a cluster are sufficiently separated that they do not interact through mutually induced viscous motions. For trichobothria clusters, it can be shown that a non-interacting-hairs assumption is reasonable if the dimensionless distance α/d between trichobothria is larger than the smallest of the pair $\{L/d, Re^{-1}\}$. For the trichobothria of *Cupiennius salei* Barth *et al.* (1993) find the following, approximate, ranges: $10 < \alpha/d < 100$, $20 < L/d < 100$ and $100 < Re^{-1} < 1000$. We must conclude from these values that hair-to-hair interactions in *Cupiennius* are probably not negligible, especially in compact trichobothria clusters with $\alpha/d < 20$. However, a more accurate analysis including mutually induced viscous motions would be very laborious to perform and one must ask if the effort is worth the reward. We eschew such an approach since

PHILOSOPHICAL TRANSACTIONS OF THE ROYAL SOCIETY B BIOLOGICAL SCIENCES

careful testing of the present model, discussed below and in Barth *et al.* (1993), shows that it accounts for all major qualitative observations and for most, if not all, quantitative observations of the motions of single hairs documented in the literature.

With the air flow field known everywhere as a function of position and time, it is possible to obtain the relative velocities and accelerations perpendicular and parallel to the respective hair segments, L_1 and L_2. In both cases of interest, shown in figures 2 and 3, the far field velocity is given by $U_o \sin(\omega t)$ denoting an oscillatory motion with zero mean net flow in the oscillation direction, and substrate curvature affects the values of the air velocity components near the substrate. On the substrate itself, the zero-velocity or 'no-slip' boundary condition applies.

Henceforth, in this communication, the substrate–air flow relative orientation shown in figure 2 will be referred to as the 'parallel flow' orientation, while that shown in figure 3 will be referred to as the 'perpendicular flow' orientation. For the parallel flow orientation we expect the radial (U) and the circumferential (V) velocity components to be $U = V = 0$ and the longitudinal component (W) to be of the general form

$$W = f_1(R,\tau;\, Re_S, St_S). \tag{21}$$

In contrast, for the perpendicular flow orientation we expect the longitudinal component of velocity to be $W = 0$ and the radial and circumferential components to be of the general form

$$U = f_2(R,\Theta,\tau;\, Re_S, St_S), \tag{22a}$$

$$V = f_3(R,\Theta,\tau;\, Re_S, St_S). \tag{22b}$$

In these equations the physical components of air velocity (u,v,w) have been non-dimensionalized according to $U = u/U_o$, $V = v/U_o$, and $W = w/U_o$. The quantities

$$Re_S = \frac{D/2\ U_o}{\nu} \qquad \text{and} \qquad St_S = \frac{\omega\ D/2}{U_o}$$

are the Reynolds and Strouhal numbers of the cylindrical substrate, respectively. They are the only dimensionless parameters required to completely characterize the velocity distributions of air oscillating parallel to, or perpendicular to, a smooth fixed cylinder of effective diameter D. The quantity $R = r/D/2$, not to be confused in the present context of writing with the damping constant R in equation (1), is the radial coordinate location along a direction perpendicular to the substrate, non-dimensionalized by the effective radius of the substrate. In equations (22*a*,*b*), Θ denotes the angular or circumferential coordinate dependence of U and V, respectively, for the perpendicular flow orientation. For this configuration the convention is that at the start of an oscillation cycle $\Theta = 0°$ along the symmetry plane that divides the flow approaching the cylinder surface, while $\Theta = 180°$ lies in the prolongation of this plane diametrically through the cylinder. From then on these angular positions are fixed, regardless of the flow reversals that occur in the oscillation cycles. As in equation (19), the quantity $\tau = \omega t$ is dimensionless time.

Completely general steady-periodic solutions of the type expressed abstractly by equations (21) and (22a,b) can be derived analytically and are relatively easy to evaluate numerically. These are discussed below.

(*a*) *Air motion parallel to the substrate axis*

This is the flow configuration shown in figure 2, in which the fluid oscillates parallel to the longitudinal axis of the cylindrical substrate. The substrate is assumed to be long enough for end effects to be ignored and $U = 0$ and $V = 0$. The equation governing the dimensionless longitudinal component of air velocity, $W(R,\tau)$, is

$$St_S \frac{\partial W}{\partial \tau} + \frac{1}{2}\frac{\partial P}{\partial Z} = \frac{1}{Re_S}\frac{1}{R}\frac{\partial}{\partial R}\left(R\frac{\partial W}{\partial R}\right), \tag{23}$$

where τ and R are defined above, $Z = z(D/2)$ and P is the non-dimensional pressure, given by $P = p/(1/2\ \rho U_o^2)$. The solution of this equation, subject to the boundary conditions that $W = 0$ at $R = 1$ and $W \to U_o \sin(\omega t)$ as $R \to \infty$, can be obtained as the sum of two parts, the first being a potential flow solution and the second being a viscous flow solution. The result is

$$W(R,\omega t) = \sin(\omega t) + \text{REAL}\,[i\,(K_0\,(\lambda R)/K_0\,(\lambda))\,e^{(i\omega t)}]. \tag{24}$$

In this equation the quantity $\lambda = (i\,Re_S\,St_S)^{1/2}$ is a known parameter and the remaining symbols have already been defined. From equation (24) it is clear that the W velocity field for this configuration is completely determined by the dimensionless parameters Re_S and St_S, through the quantity λ.

Inspection of equation (24) shows that substrate curvature affects the shape and magnitude of W through the term $K_o\,(\lambda R)/K_o\,(\lambda)$. Writing $R = 1 + y/D/2)$, with y taken as the distance from the surface of the cylindrical substrate to the radial position of interest in the flow, and considering the case when $\lambda \gg 1$ (meaning that $Re_S\ St_S \gg 1$ which is a limit of biological interest), the approximation $K_o(X) \approx e^{-X}/(2\pi X)^{1/2}$ applies, where X is a dummy variable. For these conditions equation (24) reduces to

$$W(y,t) \approx \sin(\omega t) - \frac{\sin(\omega t - \beta y)e^{-\beta y}}{(1 + y/(D/2))^{1/2}}. \tag{25}$$

Equation (25) is identical to Stokes' (1851) analytical result for a flat surface, equation (16), in the limit when $y/(D/2) \to 0$. However, as long as $Re_S\ St_S \gg 1$ the rate of exponential damping of velocity in equation (25) exceeds that due to the $(1 + y/(D/2))^{1/2}$ term and Stokes' (1851) result is expected to provide a good approximation for velocity at all values of $y/(D/2)$. We now establish what is meant in practice by $Re_S\ St_S \gg 1$.

Figure 7*a*–*c* provides comparisons among air velocity profiles calculated for the parallel and perpendicular flow orientations. Also included are the profiles for a flat substrate assuming viscous and inviscid flows,

PHILOSOPHICAL TRANSACTIONS OF THE ROYAL SOCIETY B BIOLOGICAL SCIENCES

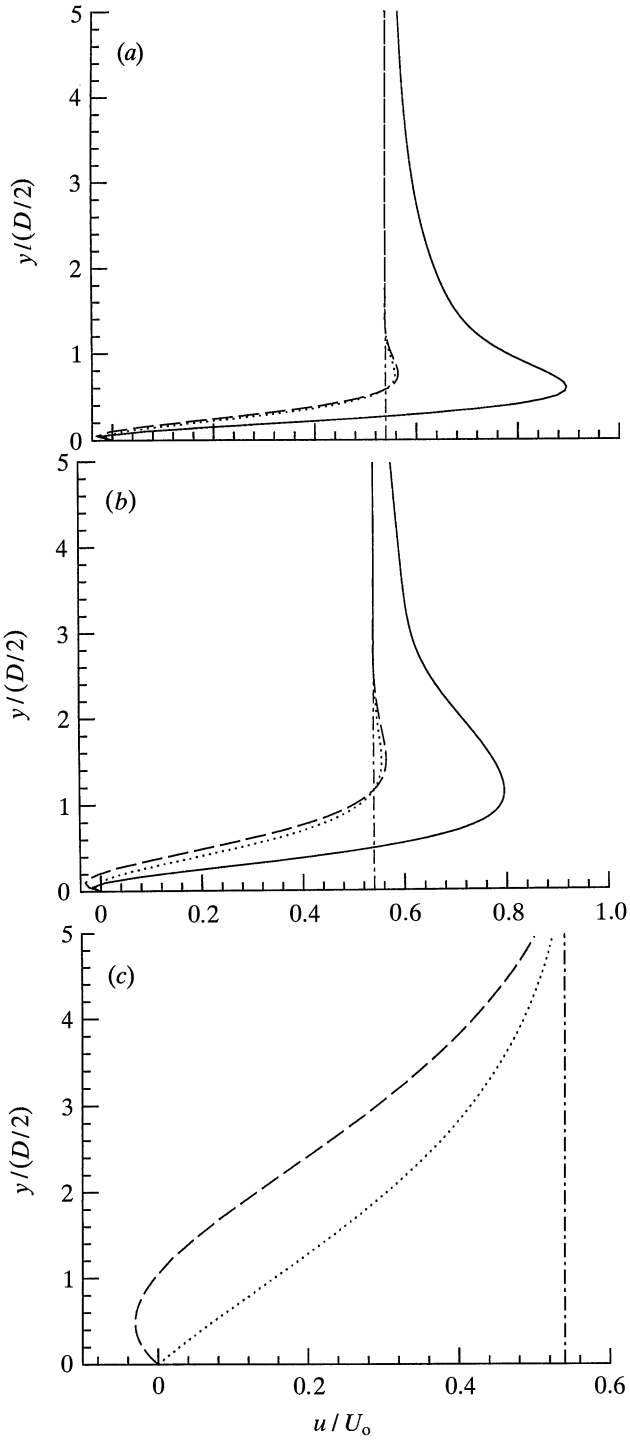

Figure 7. (*a*) Velocity profiles calculated at the same instant in time ($\omega t = 1$) in a cycle for air oscillating at $f = 100$ Hz past a cylindrical substrate with $D = 2$ mm ($Re_S St_S = 40$). Four cases shown: $u = V$ (air motion perpendicular to the cylindrical substrate) (solid line); $u = W$ (air motion parallel to the cylindrical substrate) (dotted line); $u = V_{St}$ (air motion parallel to a flat substrate, viscous flow) (dashed line); $u = U$ (air motion parallel to a flat substrate, inviscid flow) (dot-dashed line). (*b*) Velocity profiles calculated at the same instant in time in a cycle for air oscillating at $f = 100$ Hz past a cylindrical substrate with $D = 1$ mm ($Re_S St_S = 10$). The four cases shown correspond to those in (*a*). (*c*) Velocity profiles calculated at the same instant in time in a cycle for air oscillating at $f = 100$ Hz past a cylindrical substrate with $D = 0.2$ mm ($Re_S St_S = 0.4$). The three cases shown correspond to those in (*a*). The absence of the $u = V$ profile reflects that Wang's (1968) theory does not rigorously apply for $Re_S St_S < 1$.

respectively. All the results correspond to developed periodic flow at the same instant in time in an oscillation cycle, namely $\omega t = 1$. The calculation conditions listed are all biologically relevant. It is the comparison between the $u = V_{St}$ profiles, obtained from equation (16), and the curvature-affected longitudinal $u = W$ profiles, obtained from equation (24), which interests us here. For $Re_S St_S = 40$ (figure 7*a*) the two profiles are essentially the same at all times in a cycle. For $Re_S St_S = 10$ (figure 7*b*) differences begin to appear which become quite significant (in excess of 100% at $y/(D/2) = 1$) by the time $Re_S St_S = 0.40$ (figure 7*c*). These results allow us to refine the theoretical finding of the previous paragraph by taking $Re_S St_S > 10$ as the condition for Stokes' (1851) flat substrate analysis to provide a good approximation for the flow oscillating parallel to a cylindrical surface. In terms of the variables defining Re_S and St_S, this condition translates to $f D^2/\nu > 20/\pi$.

(*b*) *Air motion perpendicular to the substrate axis*

This is the flow configuration shown in figure 3, in which the fluid oscillates perpendicular to the longitudinal axis of the substrate. As in the case of the parallel flow orientation, the substrate is assumed to be long enough for end effects to be ignored and $W = 0$. Cylinders in oscillating cross-flows have been extensively investigated in the fluid mechanics literature (Telionis 1981) and the theoretical study by Wang (1968) is especially relevant here. By means of the method of inner and outer expansions this author obtained an analytical expression for the streamfunction of the instantaneous flow field at low Reynolds numbers. From this we have in turn derived an expression for the instantaneous circumferential velocity component, $V = V(R,\Theta,\tau)$, given as equation (A2.1) in Appendix 2. Although formidable in appearance, this expression is straightforward to evaluate numerically.

As expected, the perpendicular flow orientation is also completely determined by the dimensionless parameters Re_S and St_S. Figure 8, based on Wang's (1968) work for this configuration, shows four régimes of applicability of various fluid mechanic theories. The choice of theory depends on the particular values of Re_S and St_S for the cylinder. The figure provides values of Reynolds–Strouhal number pairs typical of filiform hairs and the substrates supporting them, respectively. By virtue of the regions into which the figure is subdivided, with the Reynolds and Strouhal numbers known for a particular cylinder-fluid pair, it is possible to establish the type of motion that arises as well as the simplifications allowed by the momentum equations describing that motion.

In general, the result of the interaction between an oscillating viscous flow and a circular cylinder perpendicular to that flow is the generation of a steady (in the mean) streaming motion superimposed on the unsteady component of motion. For values of Re_S $St_S < O(1)$, where the symbol 'O' denotes 'order of magnitude', the unsteady component of motion (specifically, the vorticity) is not confined to a boundary

PHILOSOPHICAL TRANSACTIONS OF THE ROYAL SOCIETY B BIOLOGICAL SCIENCES

layer immediately around the cylinder, but, instead, diffuses throughout the entire flow field. This flow régime can be further subdivided in two, according to whether inertial terms are (C) or are not (D) retained in a theoretical formulation. In the triangular region denoted (D–C) in the figure, the theories applicable to régimes (D) and (C) overlap.

When $Re_S\,St_S > O(1)$ the unsteady component of vorticity decays exponentially outside an unsteady boundary layer with thickness of $O(Re_S\,St_S)^{-1/2}$. If, in addition, $Re_S/St_S < O(1)$ (denoted as régime B, where the theory of Wang (1968) applies) the outer steady flow field is described by Stokes' (1851) theory. If, instead, $Re_S/St_S > O(1)$ (denoted as régime A) a second steady boundary layer of $O(Re_S/St_S)^{-1/2}$ arises beyond which the steady component of vorticity decays exponentially. The steady component of velocity, if it exists, is potential outside this second boundary layer.

Wang's (1968) analysis clarifies the influence of curvature terms in the equations describing both the unsteady and steady components of motion. These terms are of $O(Re_S\,St_S)^{-1/2}$, so that when $Re_S/St_S < O(1)$ (régimes B, C and D) it is necessary to retain their influence. Numerical calculations show that while the neglect of curvature terms does not seriously affect the prediction of the frequency response of filiform hairs to flow oscillations, it does lead to serious underpredictions of the magnitudes of hair displacement, velocity and acceleration, respectively. This is a most important finding since it is known that the frequency at which action potentials are generated at the base of a filiform hair depends in a complex way on the magnitudes of these quantities in addition to hair oscillation frequency (Reißland & Görner 1985).

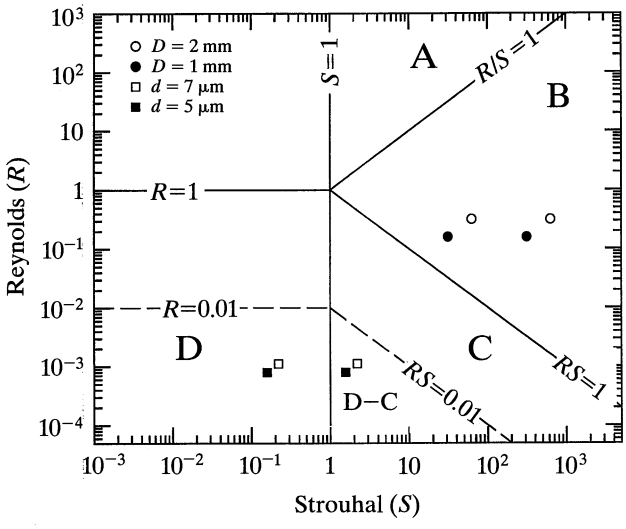

Figure 8. Map placement of Reynolds–Strouhal number pairs typical of cylindrical hairs (squares) and corresponding cylindrical substrate supports (circles) for air motions oscillating perpendicular to the substrate axis with $U_o = 5$ mm s^{-1} and frequencies ranging from 50 to 500 Hz. The regimes of applicability of the different theories are: (A) two boundary layers (Riley 1965 & Stuart 1966); (B) one boundary layer (Holtsmark *et al.* 1954; Wang 1968); (C) no boundary layer, inertia terms retained (Rayleigh 1883; Holtsmark *et al.* 1954; Lane 1955); (D) no boudary layer, inertia terms neglected (Stokes 1851); (D–C) overlap régime where (D) and (C) theories apply.

For $Re_S\,St_S \gg 1$, taking the first two terms from the binomial expansion for $(1 + y/(D/2))^2$, equation (A 2.1) in Appendix 2 reduces to

$$V(y,t) \approx \sin(\omega t)\,[1 + 1/(1 + 2\,y/(\mathrm{D}/2))] - \sin(\omega t - \beta y)\,\mathrm{e}^{-\beta y}\,[2 - \sqrt{2}\,y/(D/2) + 3/2\sqrt{2}\,(y/(D/2))^2]. \quad (26)$$

It is clear from this expression that the y-variation of the velocity profile for perpendicular flow is very different from its counterpart for parallel flow, given by equation (25). Further, in the limit when $y/(D/2) \to 0$ equation (26) yields

$$V(y,t) \approx 2\,[\sin(\omega t) - \sin(\omega t - \beta y)\mathrm{e}^{-\beta y}]. \quad (27)$$

Contrary to equation (25), the factor of 2 in equation (27) precludes its reduction to equation (16), even in the limit when $y/(D/2) \to 0$ for which we might expect Stokes' (1851) flat substrate solution to apply. It is clear that there exists a fundamental, curvature-dependent difference between the flow oscillating parallel to a cylindrical substrate and the same flow oscillating perpendicular to it. The magnitude of the difference is clearly reflected in the respective numerical evaluations of the two velocity profiles.

Figure 7*a*,*b* show $u = V$ component velocity profiles for air motion in perpendicular flow, calculated using Equation (A 2.1) for the same conditions as the other profiles. A comparison with the corresponding $u = V_{St}$ profiles shows that the flat substrate analysis is a very poor approximation for the curved substrate result. Also evident are the large differences in magnitude between the velocity profiles for parallel and perpendicular flow orientations which, per force, translate into proportionately large differences in the corresponding magnitudes for hair displacement, velocity and acceleration, respectively. Both the V- and W-velocity profiles in figure 7*a*,*b* demonstrate the thinning of the boundary layer region with increasing $Re_S\,St_S$, but with much steeper gradients in velocity (due to curvature effects) in the case of the perpendicular flow orientation. Finally, while steady streaming is expected to be negligibly small in the case of filiform hairs (small St_S), in principle it can contribute significantly to the flows around spider legs and cricket cerci (large St_S) and, therefore, to the net drag on the hairs they support. This is yet another feature not captured by Stokes' (1851) solution for a flat substrate, which equation (A 2.1) retains.

(*c*) *Experimental verification of analytical expressions for velocity*

The accuracy of equations (24) and (A 2.1) for the parallel and perpendicular flow orientations, respectively, was verified by reference to measurements obtained with a laser-Doppler velocimeter. The experimental procedure and a comparison between the measured and analytical velocity profiles are given in Barth *et al.* (1993). Briefly, measurements of the

maximum velocity in an oscillation cycle were obtained as a function of distance normal to the substrate consisting of a *Cupiennius* spider leg. The experiments were performed in a cylindrical chamber fixed with two loudspeakers operating in 'push-pull' mode to induce flow oscillations directed along the longitudinal (horizontal) axis of the chamber. For both the parallel and perpendicular flow orientations, the flow oscillation frequency and the magnitude of the free stream velocity were examined at two levels, to cover the ranges $10\ \mathrm{Hz} < f < 150\ \mathrm{Hz}$ and $15\ \mathrm{mm\ s^{-1}} < U_o < 60\ \mathrm{mm\ s^{-1}}$. The comparison between the measurements and analytical predictions of velocity was very good, with the minor discrepancies observed explainable in terms of the finite length of the experimental substrate and some unavoidable measurement uncertainty.

4. NUMERICAL SOLUTION METHODOLOGY

The general form of the equation to be solved, equation (13), can be written as

$$\ddot{\theta} + a\ \dot{\theta} + b\ \theta = c. \tag{28}$$

This second order inhomogeneous ordinary differential equation can be reduced to an equivalent system of two first order ordinary differential equations of the type

$$\dot{\theta} = p, \tag{29}$$

and

$$\dot{p} = -a\ p - b\ \theta + c, \tag{30}$$

which must be solved subject to the initial conditions that $\theta = 0$ and $\dot{\theta} = 0$ at $t = 0$. However, the complexity of the terms in these equations renders too cumbersome their analytical solution and we have chosen a numerical approach. For this we have employed a fourth order Runge–Kutta method with an adaptive stepsize algorithm especially suited to solve this type of initial value problem (see Press *et al.* 1986). The torque calculations for T_D and T_{VM} were also performed numerically using the trapezoidal rule.

A computer code was written in the FORTRAN programming language to perform the numerical calculations. (The code is available from the first author upon request.) Among the initial data required by the code are the geometrical and physical details of the hairs, and the flow field information in terms of U_o, the substrate–air flow relative orientation and the frequency range of interest. The code calculates hair displacement, angular velocity and acceleration as functions of time, and their respective steady-periodic amplitudes as functions of the forcing frequency. The code also calculates the phase difference between the motions of any two hairs, or between a hair and the air, as a function of the forcing frequency. It can perform these calculations for the configurations shown in figures 2 and 3, as well as for the flow oscillating along a flat substrate. Situations where the physical properties of the hairs have some inherent non-linear dependence on angular displacement, velocity or acceleration can also be readily simulated. For the perpendicular flow orientation it is straightforward to calculate flow fields and hair motions for hairs at Θ locations other than the $\Theta = 90°$ case studied here.

The steady-periodic amplitudes of displacement, velocity and acceleration are obtained by comparing two consecutive peaks of displacement as a function of time. The criterion for attaining a steady-periodic solution is that the difference between peaks should be less than 1%. The phase difference between two hairs is obtained by taking the product of the angular forcing frequency with the difference in the times at which the displacement of the two hairs achieve their respective maxima.

5. A METHOD FOR DETERMINING THE PHYSICAL CONSTANTS *S* AND *R*

To solve equation (13) it is necessary to prescribe values for the torsional restoring constant, S, and the damping constant, R. These physical quantities are inherent to the hair and both are due to its mechanical connection to the substrate. In the case of S there is no ambiguity concerning this point. In the case of R, one must emphasize the difference between damping due to the mechanical attachment of the hair to the substrate (which explains the need for R) and damping by the viscous action of the air on the hair, accounted for separately by terms R_1 and R_2 in equation (13).

The only direct measurements known to us for the torsional restoring constant are the static force measurements of Shimozawa & Kanou (1984) for the filiform hairs of crickets yielding values ranging from $S = 0.21 \times 10^{-12}\ \mathrm{N\ m\ rad^{-1}}$ for a hair with $d = 0.9\ \mu\mathrm{m}$ and $L_1 = 100\ \mu\mathrm{m}$ to $S = 8.5 \times 10^{-12}\ \mathrm{N\ m\ rad^{-1}}$ for a hair with $d = 4\ \mu\mathrm{m}$ and $L_1 = 1000\ \mu\mathrm{m}$. In contrast, it appears that the damping constant, R, has never been measured, directly or indirectly. Kämper & Kleindienst (1990) give experimental plots of cricket filiform hair maximum displacement, θ_{max}, and of the phase difference between hair displacement and air velocity, $\Delta\Phi$, as a function of frequency f. Some of their data are reproduced in figure 9*a*,*b* and we have considered how they might be used to derive values for S and R.

The theoretical analyses of §§ 3*a*,*b*, respectively leading to equations (25) and (27), show that for $Re_S\ St_S > 10$ (in practice meaning $f > 100\ \mathrm{Hz}$ for the cercus of figure 9*a*,*b*) a general expression for the air velocity profile seen by the bulk of a hair projecting from a cylindrical substrate can be written as

$$V_{air} = A(\omega,y)\ \sin(\omega t). \tag{31}$$

While the form of $A(\omega,y)$ significantly affects the value of θ and, hence, θ_{max}, it does not significantly affect the value of $\Delta\Phi$. Thus, for an analysis principally aimed at evaluating $\Delta\Phi$, we ignore the y-dependence of V_{air} in equation (31) and can take

$$V_{air} = U_o\ \sin(\omega t), \tag{32}$$

where U_0 is a constant. Substituting this expression for air velocity into equation (13) and solving the resulting equation (with $L_2 = 0$ to model the straight hair of

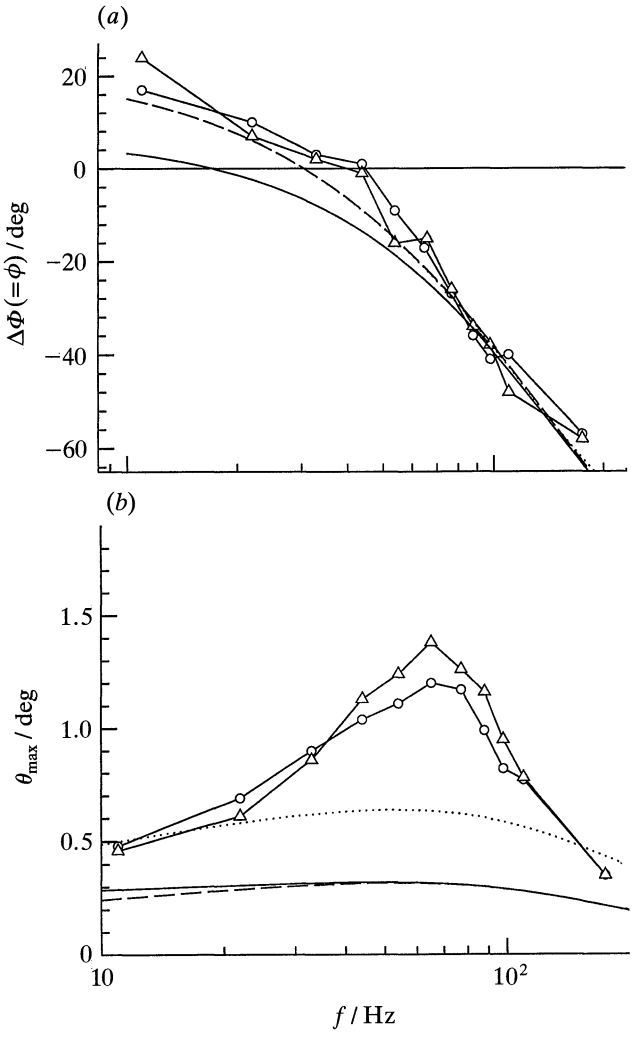

Figure 9. (*a*) Measured and calculated phase difference ($\Delta\Phi$) between hair displacement and far field air velocity plotted as a function of frequency for a straight solid hair with $L_1 = 1050$ μm and $d = 5$ μm projecting from a cylindrical substrate. Experimental data are from Kämper & Kleindienst (1990) for an air flow with $U_o = 6$ mm s^{-1}. Circles, data at 925 μm; triangles, data at 575 μm. The analytical result (solid line), based on equation (34), assumes a flat substrate and neglects viscous damping of the air motion by the substrate. The numerical results, based on equation (13), account for viscous damping of the air motion by a cylindrical substrate with $D = 1.0$ mm. Numerical solutions for the parallel substrate–air flow orientation with $U_o = 6$ mm s^{-1} (dashed line) and $U_o = 12$ mm s^{-1} (dotted line), respectively, virtually coincide. (*b*) Measured and calculated hair maximum displacement (θ_{max}) plotted as a function of frequency for the conditions of (*a*).

figure 9*a*,*b*) yields the following analytical expressions for the hair displacement, θ, and its phase shift, ϕ, respectively

$$\theta = B(\omega)\sin(\omega t + \phi), \tag{33}$$

and

$$\phi = \tan^{-1}\left[\left(1 + \frac{\pi}{4g}\frac{(S - (I + I_1)\omega^2}{(R + R_1)\omega}\right)\Big/\left(\frac{S - (I + I_1)\,\omega^2}{(R + R_1)\omega} - \frac{\pi}{4g}\right)\right]. \tag{34}$$

The analytical expression obtained for $B(\omega)$ is given by equation (A 1.7) in Appendix 1.

A comparison between equations (32) and (33) shows that the phase difference between the hair displacement and the air velocity is $\Delta\Phi = \phi$. Using the experimental data for $\Delta\Phi$ versus f given in figure 9*a*, one can choose a pair of $\Delta\Phi$ ($= \phi$) and ω ($= 2\pi f$) values which, when substituted into equation (34), yield two equations with two unknowns, S and R, as all other quantities (I,I_1,R_1, and g) are calculable. Two sets of experimental data were made available for θ_{max} and $\Delta\Phi$, respectively. The set illustrated by circles in the figures, which was measured at a distance 925 μm from the base of the hair, and the set illustrated by triangles, which was measured at a corresponding distance of 575 μm. Because of the apparent dependence of $\Delta\Phi$ on measurement position along the hair, in our procedure we averaged the two values of $\Delta\Phi$ provided at each frequency and took these averages as better statistical indicators of the variation of $\Delta\Phi$ with ω. Next, for every possible pair of ($\Delta\Phi$,ω) falling above $f = 100$ Hz in figure 9*a* we calculated the corresponding values of S and R using equation (34). For this we set $d = 5$ μm and $L_1 = 1050$ μm, corresponding to the hair dimensions for the data provided. The results for S and R were then averaged in turn, to yield final values of $S = 28.07\ \ 10^{-12}$ N m rad^{-1} and $R = 22.20\ 10^{-14}$ N m s rad^{-1}. This value of S is roughly four times that measured by Shimozawa & Kanou (1984) for a hair with similar dimensions. Given that the range of values for S measured by Shimozawa & Kanou (1984) spans two decades, and given the uncertainties affecting the measurements and procedures of both the experiments of Shimozawa & Kanou (1984) and Kämper & Kleindienst (1990), the factor of four between the two values of S seems reasonable.

Using the values of S and R estimated from the data of Kämper & Kleindienst (1990), equation (34) yields an analytical curve for $\Delta\Phi$ as a function of f. The result is shown in figure 9*a* where, as expected, good agreement is found with the experimental data for $f > 80$ Hz since this is where the present theoretical analysis applies. For $f < 80$ Hz the measurements and the analytical result differ significantly. To further investigate this point, we solved equation (13) numerically, using the above values of S and R together with the more accurate expression for the air velocity profile given by equation (24) for a parallel flow orientation as, in principle, this was the substrate–air flow relative orientation investigated by Kämper & Kleindienst (1990).

In the numerical calculations we set $D = 1.0$ mm as a reasonable effective substrate diameter after consultation with Kämper. Results for $\Delta\Phi$ and θ_{max} were then calculated with the far field velocity in equation (24) set to $U_o = 6$ mm s^{-1}, the experimental condition. For this case, the $\Delta\Phi$ profile shows much better

agreement with the corresponding measurements when $f < 80$ Hz, indicating the importance of accounting for the correct air velocity profile shape at low frequencies. In contrast, while the analytical, numerical and experimental resonance frequencies for θ_{max} (figure 9*b*) lie within less than 30% of one another, both the analytically and numerically calculated magnitudes of θ_{max} differ by about 75% from the experimental values at the measured resonance frequency ($f \approx 66$ Hz). Numerical calculations show that part of this difference can be reduced by decreasing S. However, we suspect that a much larger part of the difference is due to a departure in the experiment from the parallel flow condition assumed in the mathematical model. While it is true that the orientation of the cercus and its support were parallel to the flow direction in the experiment of Kämper & Kleindienst (1990), in practice the cercus and its support are truncated objects of finite length. Thus, in reality the flow of air past these two objects must accelerate in their vicinity, just as explained in § 3*b* for the case of a flow oscillating perpendicular to a cylindrical substrate. This effect is not captured by equation (24) and leads to an underestimation of the true air velocity near the substrate. To illustrate the influence of this on θ_{max}, numerical calculations were repeated with $U_o = 12$ mm s^{-1} in the parallel flow orientation. The results, plotted in figures 9*a*,*b*, show that doubling the far field velocity substantially improves the calculations of θ_{max} without affecting the agreement already obtained with $\Delta\Phi$.

To attempt to provide a better description of the flow past a truncated substrate mounted on a finite support was beyond the scope of this study. We note that, as expected, both the analytical and numerical calculation approaches produce resonance frequency information that is not affected by inaccuracies in the magnitudes or shapes of the air velocity profiles. In contrast, correct calculations of the magnitudes of hair displacement, velocity and acceleration require complete and physically correct prescriptions of the air velocity profiles.

At high frequencies equation (34) can be used to check the consistency of measurements obtained for $\Delta\Phi$, S and R. In future work, aimed at providing experimental information for $\Delta\Phi$ from which to calculate S and R using equation (34), special attention should be paid to making the measurements for the condition $Re_S\, St_S > 10$ for the substrate. (In practice this translates to $f > 100$ Hz, approximately, for filiform hairs on cricket cerci, and $f > 10$ Hz for trichobothria on the legs of *Cupiennius salei* spiders.) This is because for this condition only will the relative orientation of the substrate with respect to the air direction be immaterial for determining $\Delta\Phi$. Accurate measurements for the diameters and lengths of the hair substrate and its mechanical support are necessary to calculate the correct shapes and magnitudes of the air velocity profiles. Similarly, accurate measurements for hair length, diameter and shape, for the air oscillation frequency, and for the phase shift $\Delta\Phi$ are indispensable for the use of equation (34) to determine S and R. In particular, $\Delta\Phi$ should be measured as precisely as possible for values of $\Delta\Phi > 45°$ since a small error in this quantity translates into a large error in $\tan(\phi)$ and, therefore, in the values derived for S and R. For example, assuming negligible uncertainties in the values of f, d and L_1 in equation (34), we find that the uncertainty in $\Delta\Phi$ must be kept smaller than $\pm$ 5% if the uncertainties in S and R are to remain smaller than $\pm$ 10%, approximately. This is a rather stringent requirement. For the data of Kämper & Kleindienst (1990) at $f = 176$ Hz it translates into $\pm$ 3°, corresponding to a maximum allowable uncertainty in the measurement of time (from which $\Delta\Phi$ is determined) of approximately $\pm$ 5 10^{-5} s.

6. CALCULATED RESULTS AND DISCUSSION: PARAMETER DEPENDENCE OF HAIR MOTION

In this section we present and discuss numerical results calculated for several specific hair-substrate dimensions and air flow conditions. Prior to using the numerical model based on equation (13) to generate these results, we performed extensive checks to verify the goodness of the computer program encoding and the physical model itself. For example, for identical problem conditions we successfully compared the results of a numerical calculation for the case of a straight hair on a flat substrate with the corresponding viscous flow solution given in Appendix 1. We also verified that the automatic time-step adaptation algorithm was capable of yielding accurate results over the entire range of frequencies investigated. Additional verifications and self-consistency tests, not reported here but critical for verifying the goodness of the numerical procedure, were conducted in the course of this work.

Applying the methodology described in § 5 to the experimental hair-air phase difference data of Kämper & Kleindienst (1990), we obtained values for S and R appropriate to the filiform hair on a cricket cercus. The same approach could be used to obtain corresponding values of S and R for a trichobothrium but, unfortunately, the phase data are not presently available. For the calculation purposes of this section we have preferred to set $R = 0$ and have scaled the data for S obtained by Shimozawa & Kanou (1984) for the filiform hairs of crickets to yield a value of $S = 4 \times 10^{-12}$ N m rad^{-1} which we consider to be representative of spider trichobothria in both parallel and perpendicular flow orientations. However, because this choice for the S and R pair is somewhat arbitrary, we have performed an evaluation of the sensitivity of calculations for θ, $\dot{\theta}$ and $\ddot{\theta}$ to changes in these two physical constants. Additional calculations and further discussion concerning the practical importance of specifying correct values for S and R are given in the companion paper by Barth *et al.* (1993).

For all cases in the calculations to follow, the amplitude of the far-field air flow oscillations was set to $U_o = 5$ mm s^{-1}. Therefore, any differences between flow fields are due solely to substrate-air flow relative orientation effects.

PHILOSOPHICAL TRANSACTIONS OF THE ROYAL SOCIETY B BIOLOGICAL SCIENCES

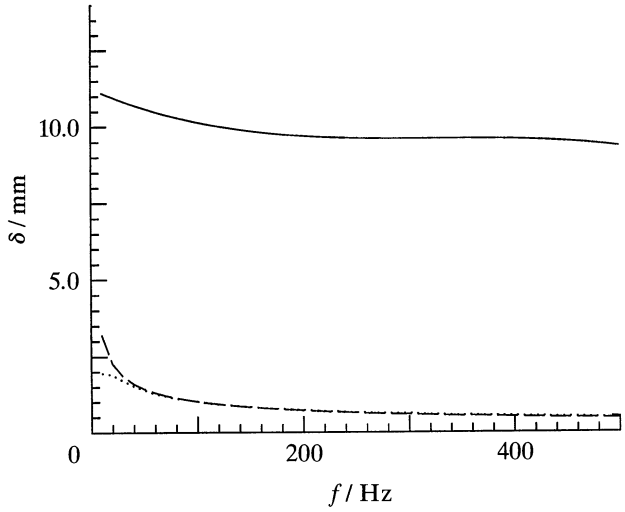

Figure 10. Boundary layer thickness (δ) as a function of frequency for cylindrical substrates with $D = 2$ mm in oscillating air flows with $U_o = 5$ mm s^{-1}; δ_{per} (air motion perpendicular to the substrate axis) (solid line); δ_{par} (air motion parallel to the substrate axis) (dotted line); δ_{St} (air motion parallel to a flat substrate) (dashed line). The profiles for δ_{par} and δ_{St} are virtually indistinguishable.

(*a*) *Sensitivity to substrate–air flow relative orientation*

In § 3 we discussed the effects of the cylindrical substrate on the oscillatory motion of air for parallel and perpendicular flow orientations. The main conclusions, substantiated by the profiles shown in figure 7*a–c* were that: (i) when $Re_S\, St_S > 10$ the results from Stokes' (1851) flat substrate analysis approximate well the flow oscillating parallel to a cylindrical surface; (ii) the flat substrate analysis never applies to the flow oscillating perpendicular to a cylindrical substrate; and (iii) the magnitude of the velocity arising in the vicinity of a cylindrical substrate for the case of perpendicular flow is always significantly larger than the corresponding value for parallel flow.

Figure 10 shows calculated boundary layer thicknesses for parallel and perpendicular flow orientations for the frequency range $10 < f(\mathrm{Hz}) < 500$. As expected, Stokes' (1851) flat substrate result, given by equation (17), is in excellent agreement with the numerically derived result for parallel flow obtained using equation (24). In contrast, the boundary layer thickness for the case of perpendicular flow, based on equation (A 2.1), is an order of magnitude larger than the value for parallel flow over the entire range of frequencies. It is clear that, of the two, the perpendicular orientation has a much more pronounced effect on both the magnitude and distribution of the flow past the substrate. For example, at 200 Hz, a 1500 μm trichobothrium would protrude significantly through the boundary layer of a parallel flow but would remain entirely immersed within the boundary layer of a perpendicular flow. Thus, for present conditions involving perpendicular flow, it is not atypical for even the longest hairs not to be exposed to the uniform far-field motion and, instead, to experience strong variations in velocity which affects their drag.

The sensitivity of the boundary layer thickness to substrate–air flow relative orientation raises a serious question concerning the validity of oversimplified analyses based on the flat substrate assumption. Thus, for example, we must reconsider the argument proposed by Fletcher (1978) that, because $\delta_{St} \approx f^{-1/2}$ in equation (17) for the flow oscillating along a flat substrate: 'Clearly for good response the hair receptor must have a length L substantially greater than δ_{St}.' That this is not true for the trichobothria of *Cupiennius salei* spiders is experimentally verified and discussed in Barth *et al.* (1993).

To illustrate the substrate orientation effect on hair motion, we have calculated the response of a straight solid trichobothrium with $d = 7$ μm and $L_1 = 500$ μm to an air flow with $U_o = 5$ mm s^{-1} in the frequency range $50 < f(\mathrm{Hz}) < 500$, corresponding to $20 < Re_S\, St_S < 200$. For the substrate we took $D = 2$ mm as a characteristic value for the diameter of a *Cupiennius* spider leg. Except for the low value of velocity used here, these conditions are typical of those investigated by Barth *et al.* (1993). Results for the maximum hair deflection angle, angular velocity and angular acceleration (θ_{max}, $\dot{\theta}_{max}$ and $\ddot{\theta}_{max}$) are plotted in figure 11*a–c*. For each of these three quantities, the coincidence between results calculated assuming a flat substrate and a parallel flow orientation, respectively, is explained by the close agreement in the corresponding air velocity profiles (figure 7*a*,*b*). For any of these three quantities, the shapes of their profiles are similar irrespective of substrate–air flow orientation. In particular, there is virtually no difference between the maximum response frequencies predicted for θ_{max} and $\dot{\theta}_{max}$ for the parallel and perpendicular flow orientations. However, the magnitudes of these quantities, and of $\ddot{\theta}_{max}$, are always larger (by about a factor of two, as expected from the analysis in § 3*b*) for the case of perpendicular flow. The conclusion is that, for otherwise identical conditions, curvature-induced acceleration of the flow in the perpendicular orientation works to deflect a hair further and at a faster rate than in the parallel flow orientation.

(*b*) *Sensitivity to variations in* S *and* R

The sensitivity of hair motion to variations in the S and R parameters was investigated for a straight solid hair with $d = 7$ μm and $L_1 = 500$ μm. Results for θ_{max}, $\dot{\theta}_{max}$ and $\ddot{\theta}_{max}$ are plotted as a function of frequency in figure 12*a–c* for three pairs of (S,R) values. Two of these pairs had $R = 0$ with $S = 3 \times 10^{-12}$ and $S = 4 \times 10^{-12}$ N m rad^{-1}, to investigate the S dependence. The third pair had $R = 1 \times 10^{-15}$ N m s rad^{-1} and $S = 4 \times 10^{-12}$ N m rad^{-1} to investigate the R dependence. The results are for a perpendicular flow orientation and they reveal a significant dependence of θ_{max}, $\dot{\theta}_{max}$ and $\ddot{\theta}_{max}$ on both S and R. For example, a 25% increase in S produces a decrease of 16% in θ_{max}. More general, however, are the following observations. With S fixed, increasing R decreases θ_{max}, $\dot{\theta}_{max}$ and $\ddot{\theta}_{max}$ at all frequencies. With R fixed, increasing S also

PHILOSOPHICAL TRANSACTIONS OF THE ROYAL SOCIETY B BIOLOGICAL SCIENCES

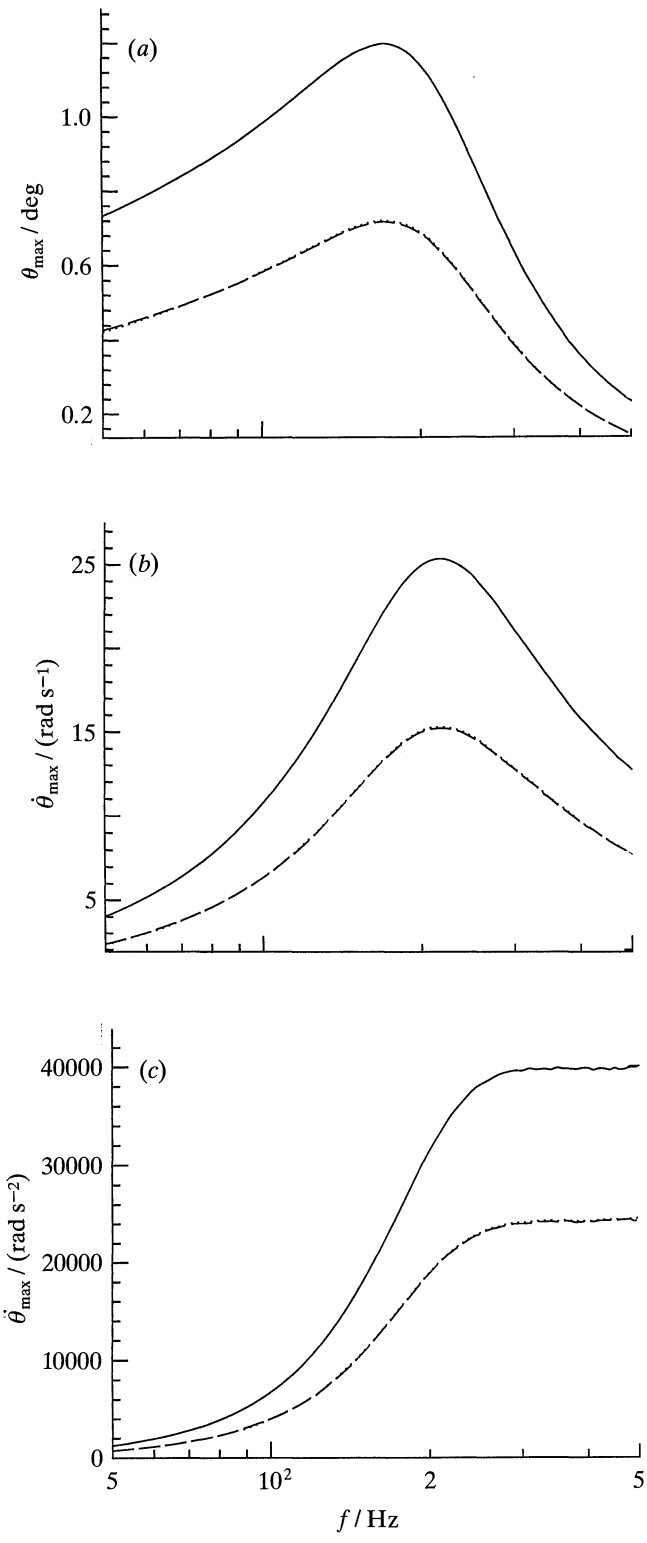

Figure 11. Sensitivity of hair motion to substrate–air flow relative orientation. (*a*) Plots of the maximum calculated displacement (θ_{max}) of a straight solid hair as a function of frequency for parallel (dashed line) and perpendicular (solid line) substrate-air flow orientations and for a flat substrate (dotted line). In the calculations: $d = 7$ μm, $L_1 = 500$ μm, $S = 4 \times 10^{-12}$ N m rad^{-1}, $R = 0$, $D = 2$ mm and $U_o = 5$ mm s^{-1}. The parallel flow and flat substrate results are virtually indistinguishable. (*b*) Plots of the maximum calculated angular velocity ($\dot{\theta}_{max}$) for the same hair and flow conditions of (*a*). (*c*) Plots of the maximum calculated angular acceleration ($\ddot{\theta}_{max}$) for the same hair and flow conditions of (*a*).

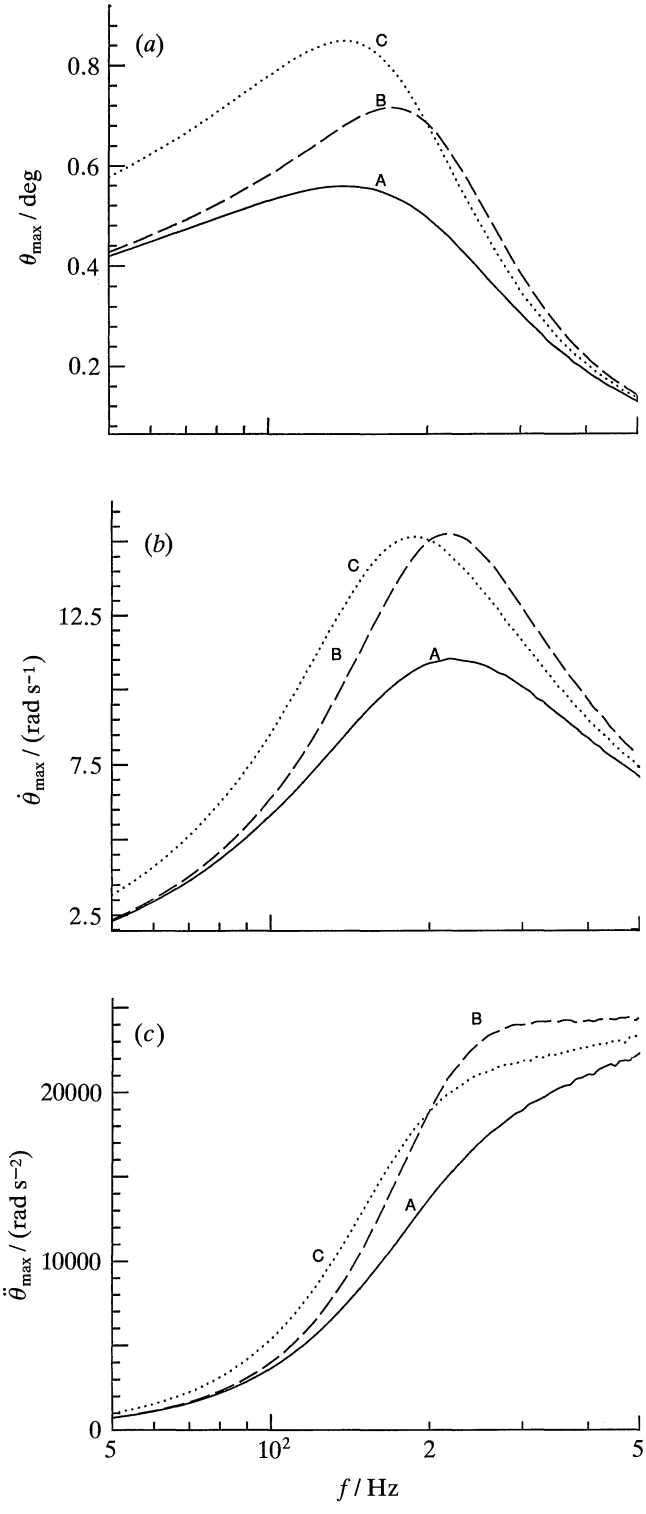

Figure 12. Sensitivity of hair motion to values of the torsional restoring constant, S, and the damping constant, R, inherent to the hair. Solid line (A), $R = 1 \times 10^{-15}$ N ms rad^{-1}, $S = 4 \times 10^{-12}$ N m rad^{-1}; dashed line (B), $R = 0$, $S = 4 \times 10^{-12}$ N m rad^{-1}; dotted line (C), $R = 0$, $S = 3 \times 10^{-12}$ N m rad^{-1}. (*a*) Plots of the maximum calculated displacement (θ_{max}) of a straight solid hair as a function of frequency. In the calculations: $d = 7$ μm, $L_1 = 500$ μm, $D = 2$ mm and $U_o = 5$ mm s^{-1} for a perpendicular substrate–air flow orientation. (*b*) Plots of the maximum calculated angular velocity ($\dot{\theta}_{max}$) for the same hair and flow conditions of (*a*). (*c*) Plots of the maximum calculated angular acceleration ($\ddot{\theta}_{max}$) for the same hair and flow conditions of (*a*).

PHILOSOPHICAL TRANSACTIONS OF THE ROYAL SOCIETY B BIOLOGICAL SCIENCES

decreases these quantities but only up to a certain frequency beyond which the effect is reversed. In the present case, for the (S,R) pairs chosen, this occurs at $f \approx 200$ Hz.

The findings of this section illustrate the importance of knowing correct values for both S and R in order to predict the true magnitude and frequency characteristics of hair motion. This point is discussed further in Barth *et al.* (1993) in relation to the trichobothria calculations presented there using values of S and R determined from experiments. Because all qualitative aspects of hair motion are correctly captured by setting $S = 4 \times 10^{-12}$ N m rad^{-1} and $R = 0$, the remainder of the calculations in this study have been performed using this pair of values.

(*c*) *Sensitivity to hair length and shape*

Under this heading we have investigated the effects of hair length and hair shape (straight or bent) on hair motion. We have also looked at the dependence of hair motion on the moment of inertia of the hair by comparing the dynamical characteristics of solid and hollow hairs for otherwise identical problem conditions. The latter effect was so small that all the results provided in the study have been for solid hairs. For the bent hairs we have investigated the sensitivity to flow direction by calculating parallel and perpendicular flow orientations. The sensitivity of hair motion to the substrate–air flow relative orientation was already examined in § 6*a* for a straight hair. Here it is the additional effect of the bend in the hair that is of interest when compared with the straight hair results.

Figure 13*a–e* shows calculated values of θ_{max}, $\dot{\theta}_{max}$, $\ddot{\theta}_{max}$, the hair to air displacement ratio (Γ) and the phase difference between hair displacement and free stream air velocity ($\Delta\Phi$) for the conditions indicated. For a discussion of hair length effects we note the profiles for θ_{max} in figure 13*a* labelled A, B and C. These correspond to straight hairs with $L_1 = 250$, 500 and 750 μm, respectively, in perpendicular flow. The plots show that hair resonance frequency decreases, and the maximum value of hair displacement increases, with increasing hair length. Both of these effects are in agreement with the experimental observations of Barth *et al.* (1993) and the numerical calculations of Shimozawa & Kanou (1984). They are due to the greater (total) moment of inertia and increased drag of a long hair relative to a short one. It is interesting that in the frequency range where the θ_{max} response of a long hair falls off, that due to a shorter hair compensates. The same trends are observed in the corresponding $\dot{\theta}_{max}$ and $\ddot{\theta}_{max}$ profiles which, as expected, show higher values for their resonance frequencies. From these findings we conclude that at low frequencies ($f < 200$ Hz, approximately, for the conditions calculated) long and middle length hairs are good displacement and velocity sensors, while at high frequencies ($f > 200$ Hz) middle length and short hairs are good velocity and acceleration sensors. A related observation has been made by Shimozawa & Kanou (1984).

For a discussion on the effects of hair shape, we consider the profiles labelled A and E in the figures. Profile E corresponds to a hair with $L_1 = 500$ μm and $L_2 = 250$ μm, also in perpendicular flow. It is clear that, relative to a straight hair of equivalent length, the quantitative behavior of a bent hair in the same flow is quite different. Even more pronounced is the difference between the response of a bent hair in perpendicular flow and that of the same hair in parallel flow, profiles E and D respectively. In this case, the shift observed in the resonance frequencies for θ_{max} and $\dot{\theta}_{max}$ are due to the different moments of inertia of these two identical hairs which oscillate in very different planes (see figures 2 and 3). The calculations show that bent hairs in perpendicular flow are approximately twice as sensitive to the displacement, velocity and acceleration of the air than the same hairs in parallel flow.

The ratio of maximum hair tip displacement to the corresponding free stream air element displacement, Γ, is plotted in figure 13*d*. This was evaluated as $\Gamma = (\theta_{max} L_1)/(U_o/\omega)$. The magnitude of this ratio and the frequency at which it maximizes are seen to be strong functions of the three parameters varied (hair shape, hair length and substrate–air flow relative orientation). From their respective analyses, both Tautz (1977) and Fletcher (1978) concluded that Γ should be of order 2 for hairs oscillating near to their undamped natural frequencies. In their experiments, Kämper & Kleindienst (1990) found $0.2 < \Gamma < 2$ with the value of Γ exceeding 2 in two cases. Present calculations with the hair damping constant set to $R = 0$ and the dimensions and flow conditions shown in the figure support the 0.2–2 range of variation in Γ. However, we find for the trichobothria in Barth *et al.* (1993) that the upper limit of this range is reduced when finite values of R are used in the calculations.

Although we have restricted present considerations to the parallel and perpendicular flow orientations shown in figures 2 and 3, it should be clear that bends at the tips of trichobothria sensitize these hairs to other flow directions, especially those approaching a spider from above. In crickets, for example, directionally independent sensitivity to air flow is guaranteed by the presence of numerous straight filiform hairs circumferentially distributed around each cercus so that there are always some hairs affected by air motion. In contrast, in any cluster on a leg of a *Cupiennius* spider the trichobothria are less in number and not circumferentially distributed around the leg. Here it appears that directionally-independent sensitivity to air flow may be assisted by hair curvature. This point is further discussed in the companion paper by Barth *et al.* (1993).

(*d*) *Phase shift between hairs in a cluster*

Calculations were also performed to show the dependence of the phase difference between hair displacement and air velocity, $\Delta\Phi$, on various parameters. Figure 13*e* provides results for the hairs and conditions listed in figure 13*a*. The profiles for the

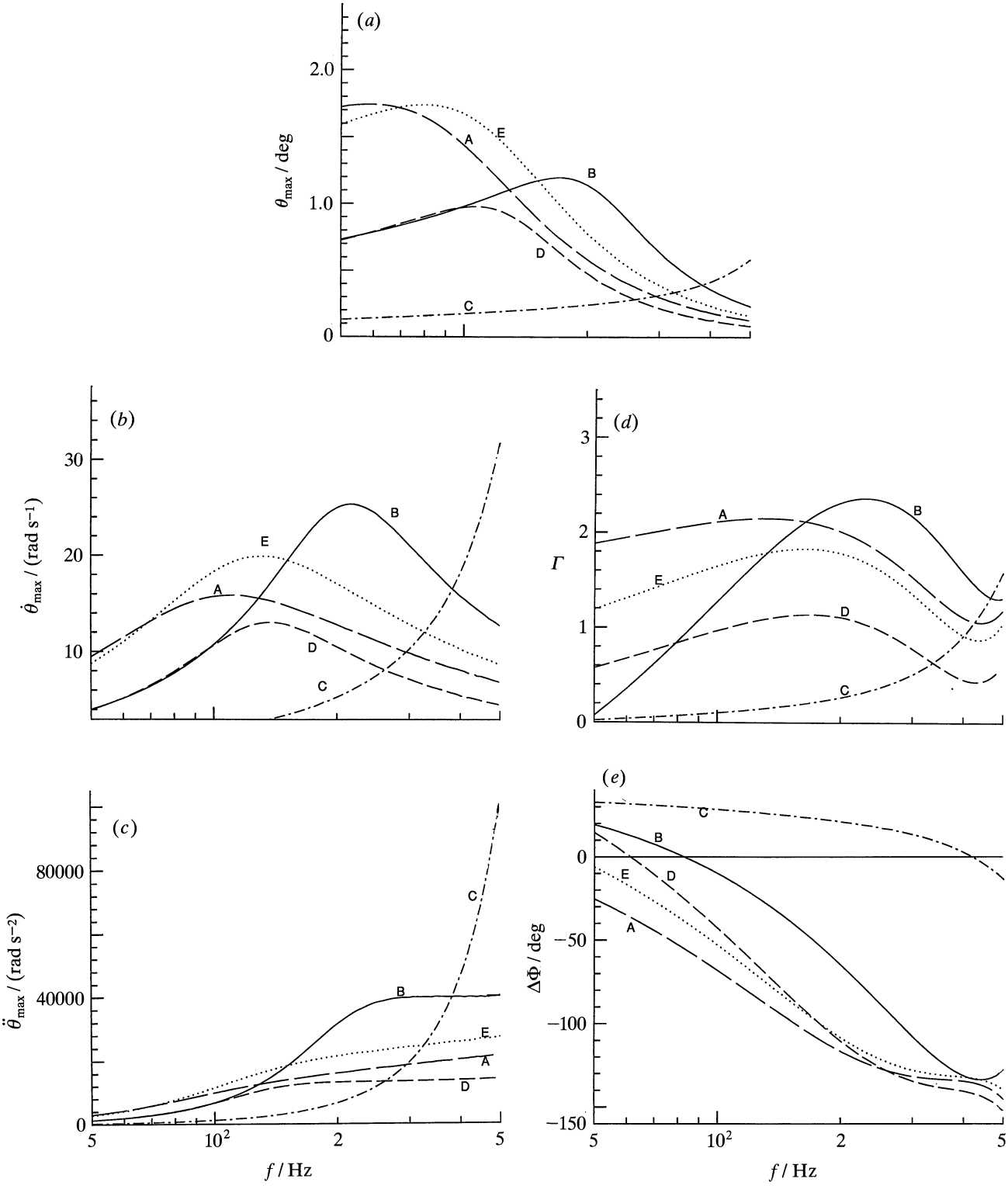

Figure 13. Sensitivity of hair motion to hair length and shape for parallel and perpendicular substrate–air flow orientations. Long-dashed line (A), perpendicular, $L_1 = 750$ μm, $L_2 = 0$; solid line (B), perpendicular, $L_1 = 500$ μm, $L_2 = 0$; dot-dashed line (C), perpendicular, $L_1 = 250$ μm, $L_2 = 0$; short-dashed line (D), parallel, $L_1 = 500$ μm, $L_2 = 250$ μm; dotted line (E), perpendicular, $L_1 = 500$ μm, $L_2 = 250$ μm. In the calculations: $d = 7$ μm, $S = 4 \times 10^{-12}$ N m rad^{-1}, $R = 0$, $D = 2$ mm and $U_o = 5$ mm s^{-1}. (*a*) Plots of the maximum calculated displacements (θ_{max}) of the solid hairs as a function of frequency. (*b*) Plots of the maximum calculated angular velocity ($\dot{\theta}_{max}$) for the same hair and flow conditions of (*a*). (*c*) Plots of the maximum calculated angular acceleration ($\ddot{\theta}_{max}$) for the same hair and flow conditions of (*a*). (*d*) Plots of the hair to air displacement ratio (Γ) for the same hair and flow conditions of (*a*). (*e*) Plots of the phase differences between hair location and air velocity ($\Delta\Phi$) for the same hair and flow conditions of (*a*).

straight hairs show that long hairs are more phase delayed than short ones, in agreement with the measurements of Kämper & Kleindienst (1990).

Taking the difference, at a fixed frequency, between any two pair of profiles in this figure yields the phase difference in displacement between the corresponding pair of hairs. Thus, for example, comparing the profiles for the same bent hair in parallel (D) and perpendicular (E) flows, we observe only a small phase difference between the two. In contrast, the calculations show large phase differences between hairs of significantly different lengths for all frequencies. This finding is of potential biological significance since such phase differences among hairs in a cluster can, in principle, significantly affect the pattern of their combined action potentials.

One of us, J.A.C.H., gratefully acknowledges financial support received from the Committee on Research of the University of California at Berkeley to pursue this investigation. J.A.C.H. is also grateful to the National Science Foundation for a Cooperative Research Award allowing travel to consult on the project with F.G.B. at the University of Vienna. The Austrian Science Foundation (FWF; P7882-B) generously supported F.G.B. with travel funds to facilitate the collaboration. Part of this study was written while F.G.B. was a Russell Severance Springer Professor during the Fall of 1991 in the Department of Mechanical Engineering at the University of California at Berkeley. We are indebted to G. Kämper and H.-U. Kleindienst for making available in tabulated form the data plotted in figure 9*a–b*. We are also indebted to S. Morris and F. S. Sherman for valuable discussions pertaining to the theoretical content of this paper.

REFERENCES

Abramowitz, M. & Stegun, I.A. 1970 *Handbook of mathematical functions*. New York: Dover Publications.

Barth, F.G., Wastl, U., Humphrey, J.A.C. & Devarakonda, R. 1993 Dynamics of arthropod filiform hairs. II. Mechanical properties of spider trichobothria (*Cupiennius salei* Keys.) *Phil. Trans. R. Soc. Lond.* B **340**, 445–461. (Following paper.)

Barth, F.G. & Blickhan, R. 1984 Mechanoreception. In *Biology of the Integument*, vol. 1 (*Invertebrates*), VIII (*Arthropoda*) (ed. J. Bereiter-Hahn, A. G. Matoltsy & K. S. Richards), pp. 554–582. Berlin: Springer-Verlag.

Fletcher, N.H. 1978 Acoustical response of hair receptors in insects. *J. comp. Physiol.* **127**, 185–189.

Holtsmark, J., Johnsen, I., Sikkeland, T. & Skavlem, S. 1954 Boundary layer flow near a cylindrical obstacle in an oscillating incompressible fluid. *J. acoust. Soc. Am.* **26**, 26–39.

Kämper, G. & Kleindienst, H.-U. 1990 Oscillation of cricket sensory hairs in a low-frequency sound field. *J. comp. Physiol.* **167**, 193–200.

Lane, C.A. 1955 Acoustic streaming in the vicinity of a sphere. *J. acoust. Soc. Am.* **27**, 1082–1086.

Panton, R.L. 1984 *Incompressible flow*. New York: John Wiley & Sons.

Press, W.H., Flannery, B.P., Teukolsky, S.A. & Vetterling, W.T. 1986 *Numerical recipes*. Cambridge University Press.

Rayleigh, Lord 1883 On the circulation of air observed in Kundt's tubes, and on some allied acoustical problems. *Phil. Trans.* **175**, 1–21. *Scient. Pap.* **2**, 239–257.

Reißland, A. & Görner, P. 1978 Mechanics of trichobothria in orb-weaving spiders (Agelenidae, Araneae). *J. comp. Physiol.* **123**, 59–69.

Reißland, A. & Görner, P. 1985 Trichobothria. In *Neurobiology of arachnids* (ed. F. G. Barth), pp. 138–161. Berlin: Springer Verlag.

Riley, N. 1965 Oscillating viscous flows. *Mathematika* **12**, 161–175.

Shimozawa, T. & Kanou, M. 1984 The aerodynamics and sensory physiology of range fractionation in the filiform sensilla of the cricket *Gryllus bimaculatus*. *J. comp. Physiol.* **155**, 495–505.

Stokes, G.G. 1851 On the effect of the internal friction of fluids on the motion of pendulums. *Trans. Camb. phil. Soc.* **9**, 8ff. (Reprinted in *Mathematical and physical papers*, vol. III, pp. 1–141. Cambridge University Press, 1901.)

Stuart, J.T. 1966 Double boundary layers in oscillatory viscous flow. *J. Fluid Mech.* **24**, 673–687.

Tautz, J. 1977 Reception of medium vibration by thoracal hairs of caterpillars of *Barathra brassicae* L. (Lepidoptera, Noctuidae) I. Mechanical properties of the receptor hairs. *J. comp. Physiol.* **118**, 13–31.

Tautz, J. 1979 Reception of particle oscillation in a medium. An unorthodox sensory capacity. *Naturwissenschaften* **66**, 452–461.

Telionis, D.P. 1981 Unsteady viscous flows. *Springer Series in Computational Physics*, New York: Springer-Verlag.

Wang, C.-Y. 1968 On high-frequency oscillatory viscous flows. *J. Fluid Mech.* **32**, 55–68.

White, F.M. 1991 *Viscous fluid flow* (2nd edn.). New York: McGraw-Hill.

Received 14 September 1992; accepted 10 December 1992

APPENDIX 1

Analysis of the motion of a straight cylindrical hair oscillating about a point on a flat immobile substrate due to an imposed periodic flow: viscous and inviscid substrate flow solutions

The equation to be solved is equation (13) in the text after setting $L_2 = 0$ and neglecting the second term contributing to F_{VM} in equation (7). Thus, the equation of interest is

$$(I + I_1)\ \ddot{\theta} + (R + R_1)\ \dot{\theta} + S\,\theta = 4\pi\,\mu\,G \int_0^{L_1} V_F\, y\, dy - \frac{\pi\mu\, G}{2\, g f} \int_0^{L_1} \dot{V}_F\, y\, dy. \quad \text{(A 1.1)}$$

(i) *Viscous flow analysis*

For the fluid velocity required in equation (A 1.1) we take equation (16) which corresponds to the viscous oscillatory motion of a fluid adjacent to a flat, immobile surface. However, to maintain a correspondence with the work of Shimozawa & Kanou (1984), instead of equation (16) we use the completely equivalent expression employed by them. This is given by

$$V_{St} = v/U_o = \cos(\omega t) - \cos(\omega t - \beta y)\ e^{-\beta y}, \quad \text{(A 1.2)}$$

where the symbols used have already been defined in the text.

Noting that $V_F = v \cos\theta$ and that for $\theta < 10°$ the $\cos(\theta) \to 1$, from equation (A 1.2) V_F and its time derivative, $\dot{V}_F$, can be found. Substituting these quan-

PHILOSOPHICAL TRANSACTIONS OF THE ROYAL SOCIETY B BIOLOGICAL SCIENCES

tities into equation (A 1.1), and reorganizing terms, yields the result

$$I_t \ddot{\theta} + R_t \dot{\theta} + S\theta = P\cos(\omega t) + Q\sin(\omega t), \quad \text{(A 1.3)}$$

where

$$I_t = I + I_1, \qquad R_t = R + R_1,$$

$$P = 2\pi\mu G U_o L_1^2 A - (\pi^2 \mu G U_o L_1^2/2g) B,$$

$$Q = 2\pi\mu G U_o L_1^2 B + (\pi^2 \mu G U_o L_1^2/2g) A,$$

with

$$A = e^{-\beta L_1}[-(1/\beta L_1)\cos(-\beta L_1) - (1/\beta L_1 + 1/(\beta L_1)^2)\sin(-\beta L_1)] - 1,$$

and

$$B = e^{-\beta L_1}[(1/\beta L_1)\sin(-\beta L_1) - (1/\beta L_1 + 1/(\beta L_1)^2)\cos(-\beta L_1)] + 1/(\beta L_1)^2.$$

The steady-peroidic solution of equation (A 1.3) is

$$\theta = C_1\cos(\omega t) + C_2\sin(\omega t), \quad \text{(A 1.4)}$$

with the constants C_1 and C_2 given by

$$C_1 = \frac{P(S - I_t\omega^2) - Q\omega R_t}{(S - I_t\omega^2)^2 + (\omega R_t)^2},$$

and

$$C_2 = \frac{P\omega R_t + Q(S - I_t\omega^2)}{(S - I_t\omega^2)^2 + (\omega R_t)^2}.$$

With analytical expressions available for V_F, θ and their respective time derivatives, it is a straightforward matter to derive corresponding expressions for T_{VM} and T_D from the definitions given by equations (3) and (4) in the text. The results are

$$T_{VM} = \frac{\pi^2\mu G L_1^2}{g}\left\{\left[-\frac{L_1}{3}C_1\omega - \frac{BU_o}{2}\right]\cos(\omega t) + \left[-\frac{L_1}{3}C_2\omega + \frac{AU_o}{2}\right]\sin(\omega t)\right\}, \quad \text{(A 1.5)}$$

$$T_D = -4\pi\mu G L_1^2\left\{\left[\frac{L_1}{3}C_2\omega - \frac{AU_o}{2}\right]\cos(\omega t) + \left[-\frac{L_1}{3}C_1\omega - \frac{BU_o}{2}\right]\sin(\omega t)\right\}. \quad \text{(A 1.6)}$$

(ii) *Inviscid flow analysis*

For the fluid velocity required in equation (A 1.1) we now take $U_o\cos(\omega t)$ for all values of y, which corresponds to the inviscid oscillatory motion of a fluid adjacent to a flat, immobile surface. The analytical solution to this problem also requires solving equation (A 1.3) where, now, $A = 1$ and $B = 0$ in the expressions for P and Q. The expressions for I_t and R_t remain as previously defined. The final steady-periodic solution is given by equation (A 1.4) with the constants C_1 and C_2 also as previously defined. To obtain the form of $B(\omega)$ required by equation (33) in the text we recast equation (A 1.4) into that form to find

$$B(\omega) = \sqrt{(C_1^2 + C_2^2)}. \quad \text{(A 1.7)}$$

APPENDIX 2

Analytical solution for the Θ component of velocity for a viscous fluid oscillating perpendicular to an immobile cylindrical substrate

Wang (1968), provides an analytical expression for the stream function, ψ, for the flow oscillating perpendicular to a fixed cylinder. For this configuration, the circumferential velocity component, V, that is, the component aligned in the Θ direction, is the one relevant to calculating hair motion. This component is obtained by taking the radial derivative of the stream function as follows

PHILOSOPHICAL TRANSACTIONS OF THE ROYAL SOCIETY B BIOLOGICAL SCIENCES

$$V_\Theta(R,\Theta,\omega t) = \partial\psi/\partial R \qquad \text{(A 2.1)}$$

$$= (1 + 1/R^2)\sin\Theta\cos\omega t + (Re_S St_S)^{-1/2}(\sqrt{2}/R^2)\sin\Theta(\sin\omega t + \cos\omega t)$$

$$+ (Re_S St_S)^{-1}(1/R^2)\sin\Theta\sin\omega t - 2\sin\Theta\, e^{-\eta/\sqrt{2}}\cos(\omega t - (\eta/\sqrt{2}))$$

$$- (Re_S St_S)^{-1/2}\sin\Theta\, e^{-\eta/\sqrt{2}}\left\{\frac{1}{\sqrt{2}}[\cos(\omega t - (\eta/\sqrt{2})) + \sin(\omega t - (\eta/\sqrt{2}))] - \sqrt{2}\,\eta\cos(\omega t - (\eta/\sqrt{2}))\right\}$$

$$- (Re_S St_S)^{-1}\sin\Theta\, e^{-\eta/\sqrt{2}}\{-1/4\sin(\omega t - (\eta/\sqrt{2})) - (5/4\sqrt{2})\,\eta[\cos(\omega t - (\eta/\sqrt{2})) + \sin(\omega t - (\eta/\sqrt{2}))] + (3/2\sqrt{2})\,\eta^2\cos(\omega t - (\eta/\sqrt{2}))\}$$

$$+ (St_S)^{-1}\sin 2\Theta\{e^{-\eta}\sin(2\omega t - \eta) + e^{-\eta/\sqrt{2}}(\eta/\sqrt{2})[\cos(2\omega t - (\eta/\sqrt{2})) + \sin(2\omega t - (\eta/\sqrt{2}))]\}$$

$$- (Re_S St_S)^{-1/2}\sin\Theta\,(e^{-\eta/\sqrt{2}}/\sqrt{2})[\cos(\omega t - (\eta/\sqrt{2})) + \sin(\omega t - (\eta/\sqrt{2}))]$$

$$+ (Re_S St_S)^{-1}\sin\Theta\, e^{-\eta/\sqrt{2}}\{-5/4\sin(\omega t - (\eta/\sqrt{2})) + (3/2\sqrt{2})\,\eta[\cos(\omega t - (\eta/\sqrt{2})) + \sin(\omega t - (\eta/\sqrt{2}))]\}$$

$$- (St_S)^{-1}\sin 2\Theta\, e^{-\eta/\sqrt{2}}\sin(2\omega t - (\eta/\sqrt{2}))$$

$$- (St_S)^{-1}\sin 2\Theta\,(3/2R^3)$$

$$+ (St_S)^{-1}\sin 2\Theta\{1/2\, e^{-\sqrt{2}\eta} + e^{-\eta/\sqrt{2}}[\cos(\eta/\sqrt{2}) + 5\sin(\eta/\sqrt{2})]\}$$

where $\eta = (Re_S St_S)^{1/2}(R - 1)$ and $R = 1 + (y/(D/2))$, respectively.